

# The Boundary Time Crystal as a light source for quantum enhanced sensing beyond the Heisenberg Limit

Malik Jirasek,<sup>1</sup> Igor Lesanovsky,<sup>1,2</sup> and Albert Cabot<sup>1</sup>

<sup>1</sup>*Institut für Theoretische Physik, Universität Tübingen,  
Auf der Morgenstelle 14, 72076 Tübingen, Germany*

<sup>2</sup>*School of Physics and Astronomy and Centre for the Mathematics  
and Theoretical Physics of Quantum Non-Equilibrium Systems,  
The University of Nottingham, Nottingham, NG7 2RD, United Kingdom*

Modern precision measurements, such as interferometry for detecting gravitational waves, rely on the estimation of optical phases encoded in light fields. Here, we propose to exploit the collectively enhanced output field of a driven-dissipative many-body open quantum system as a light source in order to improve the precision of estimating optical phases. Pronounced temporal correlations of such output fields benefit the sensitivity of measurement protocols, which we show theoretically by employing a boundary time crystal as a light source. The fundamental bound on the precision of such estimation shows scaling with system size that surpasses the Heisenberg limit and obeys the standard quantum limit in the measurement time. This scaling can be partially harnessed by a protocol, in which the phase shifted light field is guided into an auxiliary replica system, which serves as a detector that is sensitive to non-trivial temporal correlations of the light.

*Introduction.*— Quantum technologies promise sensors that surpass the precision of their traditional counterparts, for example in magnetometry [1] or interferometry for the detection of gravitational waves [2]. Sensing applications might also benefit from novel light sources that rely on the exploitation of collective phenomena in driven-dissipative quantum systems [3, 4]. These may feature steady state superradiance [3, 4], synchronization [5, 6], or time crystal phases [7–9], that influence the properties of their light emission. In the case of time crystal phases, their characteristic asymptotic oscillatory behavior [10–12] leads to persistent temporal correlations in their emitted light [8, 13]. These oscillations occur either with a period that is a discrete multiple of that of an external driving [9, 14–26], or with a period varying continuously with system parameters, in the case of time-independent driving [7, 27–39]. An example of the latter case is the boundary time crystal (BTC) [7], emerging in driven-dissipative collective spin systems, as those realized in dense pencil-shaped atomic clouds [40]. In its stationary regime, the BTC light output displays the same statistics as the laser driving it, while in its time crystal regime, the light output exhibits intricate time-correlations which become more pronounced with system size [8, 13].

In this paper we investigate, how a BTC can be exploited as a source of light that enables quantum enhanced parameter estimation. In particular, we consider the setting depicted in Fig. 1(a), in which the output light is used to measure an external phase shift  $\varphi$  imprinted by a sample. Note, that this use case is conceptually different to many recent studies which aim to estimate unknown parameters that govern the BTC evolution itself [41–46]. The fundamental precision with which the emitted light permits the determination of the phase shift is quantified by the quantum Fisher information (QFI)

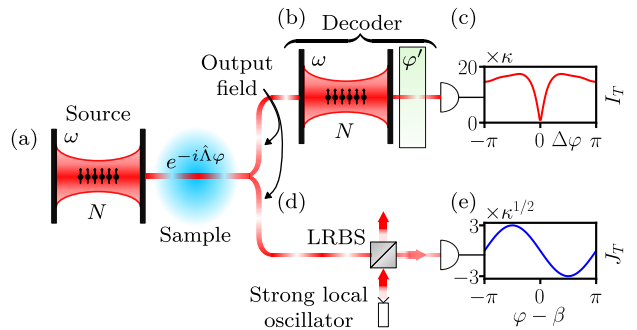


FIG. 1. **The boundary time crystal as a light source.** (a) The emission field of a boundary time crystal (BTC) composed of  $N$  emitters and driven with Rabi frequency  $\omega$  is used as a resource for probing an unknown sample. The sample encodes a phase  $\varphi$  on the output field, which is described by the unitary  $e^{-i\hat{\Lambda}\varphi}$ , with the photon count operator  $\hat{\Lambda}$ . (b) An auxiliary, identical BTC with a tunable phase shift  $\varphi'$  imprinted on its output is used as a decoder for the information encoded on the output field. (c) The output time averaged intensity  $I_T$  of the source-decoder system is monitored and is sensitive to the phase difference  $\Delta\varphi = \varphi - \varphi'$ . For  $\Delta\varphi = 0$ , the average intensity vanishes, rendering the decoder a perfect absorber for the phase shifted input light. Values presented are computed for  $N = 6$  and  $\omega/\omega_c = 4$ . (d) The output field is superposed with the field of a strong local oscillator in a homodyne detection scheme, using a low reflectivity beam splitter (LRBS) with homodyne phase  $\beta$ . The indicated output port is monitored, yielding the homodyne current  $J_T$  which is sensitive to the phase difference  $\varphi - \beta$ , for which results are presented in (e) for  $N = 6$  and  $\omega/\omega_c = 0.5$ .

of the source system and its output field [47, 48]. This QFI scales with  $N^4$  in the system size  $N$  of the BTC in the time crystal regime, which is stronger than Heisenberg scaling with  $N^2$  displayed in the stationary regime. In order to tap the quantum enhancement anticipated by the QFI, we propose two different measurement protocols to retrieve the information about  $\varphi$  encoded in the BTC

output light. The first protocol is akin to homodyne detection [6, 44, 49–62] [see Fig. 1(d)–(e)], while in the second protocol, the emitted light of a BTC is guided into an auxiliary replica system acting as a decoder for the phase shifted light [63, 64] [see Fig. 1(b)–(c)]. We show, that both protocols saturate the quantum Cramér-Rao bound (QCRB) in the stationary regime and thus the estimation error of the measured phase shift  $\delta\varphi$  displays Heisenberg scaling in the system size. In the time crystal regime, the second protocol achieves scaling of the phase estimation error as  $\delta\varphi \propto 1/N^{1.222}$ , which exceeds the Heisenberg limit.

*Fundamental bounds on precision.*— To set the stage, we briefly introduce the ultimate limit on precision with which an external phase shift can be measured, using a dissipative many-body quantum system as a light source. The dynamics shall be described by a Lindblad master equation ( $\hbar = 1$ )

$$\partial_t \rho = -i[\hat{H}, \rho] + \kappa \mathcal{D}[\hat{L}]\rho =: \mathcal{L}[\rho], \quad (1)$$

with the dissipator  $\mathcal{D}[\mathcal{O}]\rho = \mathcal{O}\rho\mathcal{O}^\dagger - \{\mathcal{O}^\dagger\mathcal{O}, \rho\}/2$  and the density matrix reduced to the system  $\rho$ . The Hamiltonian  $\hat{H}$  describes coherent processes, for instance the coherent driving of the source system by the light inside a cavity as illustrated in Fig. 1(a). The jump operator  $\hat{L}$  describes the emission of a photon by the source system with the corresponding rate  $\kappa$  into an environment, for example out of the cavity into a waveguide. In the input output formalism [65], the global state of system and environment is a matrix product state (MPS)  $|\psi_\varphi\rangle$  [47, 48, 63]. When guided through an unknown sample, the light emitted by the source system acquires a phase shift  $\varphi$  [see Fig. 1(a)], which is described by the unitary transformation  $|\psi_\varphi\rangle = e^{-i\hat{\Lambda}\varphi}|\psi_0\rangle$  [48]. Here the state  $|\psi_0\rangle$  is the global state in absence of a phase shift, and  $\hat{\Lambda}$  is the photon count operator (see Supplemental Material (SM) [66] for details). Effectively, the unitary transformation of the global state can be expressed as a transformation of the system jump operator corresponding to the emission of a photon  $\hat{L} \rightarrow e^{-i\varphi}\hat{L}$  [48].

As a figure of merit for the performance of a measurement of the parameter  $\varphi$ , we consider the estimation error  $\delta\varphi$ . This is formally given by the standard deviation of an unbiased estimator specific for a given measurement protocol [42, 67–69]. Optimizing over all possible measurements yields the quantum Cramér-Rao bound (QCRB) for the estimation error [68, 69]

$$\delta\varphi \geq \frac{1}{\sqrt{F_\varphi(\varphi_0, T)}}, \quad (2)$$

where  $F_\varphi(\varphi_0, T)$  is the QFI of the system and environment state for estimating  $\varphi$ , evaluated at the actual parameter value  $\varphi_0$  and measurement time  $T$  [47, 48]. In the limit of long measurement times, one finds linear growth of the QFI with the measurement time, such that

the QFI rate  $f_\varphi := \lim_{T \rightarrow \infty} F_\varphi(\varphi_0, T)/T$  only depends on the system parameters and the estimated phase shift  $\varphi$ . By employing the MPS description of the global system and environment state we further find the long-time QFI rate [66]

$$f_\varphi = \frac{8\kappa^2}{T} \int_0^T dt \int_0^{T-t} d\tau C(\tau) + 4\kappa \langle \hat{L}^\dagger \hat{L} \rangle_{\text{ss}} - 4\kappa^2 T \langle \hat{L}^\dagger \hat{L} \rangle_{\text{ss}}^2, \quad (3)$$

where  $C(\tau) := \text{Tr}[\hat{L}^\dagger \hat{L} e^{\mathcal{L}\tau} (\hat{L} \rho_{\text{ss}} \hat{L}^\dagger)]$  and  $\langle \mathcal{O} \rangle_{\text{ss}} = \text{Tr}[\mathcal{O} \rho_{\text{ss}}]$  with the stationary state  $\rho_{\text{ss}}$ . This shows, that the QFI rate is essentially given by the time integrated two-time intensity correlation of the system output [48, 69] and independent of the actual parameter value  $\varphi_0$ .

*The Boundary Time Crystal as a light source.* — In the following, we consider the BTC as the light source. The BTC is a system composed of  $N$  two level emitters. It features collective resonant driving with Rabi frequency  $\omega$  and collective dissipation with rate  $\kappa$ , described by the Hamiltonian  $\hat{H} = \omega \hat{S}_x$  and the jump operator  $\hat{L} = \hat{S}_-$ , respectively. The operators  $\hat{S}_\alpha = \sum_{i=1}^N \hat{\sigma}_\alpha^i/2$ , with  $\alpha \in \{x, y, z\}$ , are collective total angular momentum operators, where the Pauli matrices  $\hat{\sigma}_\alpha^i$  correspond to emitter  $i$ , and the ladder operators are  $\hat{S}_\pm = \hat{S}_x \pm i\hat{S}_y$ . Such a system can be realized experimentally [40] and has been discussed extensively in the literature [7, 8, 13, 27]. It features a phase transition in the thermodynamic limit ( $N \rightarrow \infty$ ) from a stationary regime to a time crystal regime. The transition occurs at the critical Rabi frequency  $\omega_c = N\kappa/2$  [13], which implies that Rabi frequencies have to be adjusted with system size when considering fixed values of  $\omega/\omega_c$ . For  $\omega < \omega_c$ , the system displays a stationary regime and rapidly approaches a stationary state via overdamped relaxation [8, 13]. For  $\omega > \omega_c$ , the system is in a time crystal regime, characterized by oscillating system observables [8, 13].

We determine the bound on the phase estimation error  $\delta\varphi$  with a BTC as a light source. To calculate this, we have to compute the QFI rate Eq. (3) for both the stationary and time crystal regimes of the BTC. In the stationary regime, a Holstein-Primakoff (HP) approach yields  $f_\varphi \approx 4\omega^2/\kappa$  [66]. Assuming constant ratios  $\omega/\omega_c$ , this yields an  $N^2$  scaling of the QFI rate in this regime. Deep in the time crystal regime ( $\omega/\omega_c \gg 1$ ), we compute the correlation function  $C(\tau)$  analytically by using the superspin method [45, 70], resulting in the long-time QFI rate [66]

$$f_\varphi \approx \kappa N(N+2) \left[ \frac{(N-1)(N+3)}{135} + \frac{2}{3} \right] =: f_{\varphi,\infty}, \quad (4)$$

where the approximation becomes exact when  $\omega/\omega_c \rightarrow \infty$ . This shows, that the sensitivity of the BTC light for measuring optical phases is enhanced by pronounced temporal correlations of the output field in the time

crystal regime. These correlations grow with the number of emitters in the BTC [13], leading to a scaling of  $f_{\varphi,\infty} \propto N^4$  for large, but finite system sizes. In the SM [66], we benchmark these analytical expressions with the numerical calculation of  $f_{\varphi}$ , finding that they capture accurately the scaling behavior of the long-time QFI rate in both dynamical regimes.

*Average homodyne current protocol.*— Whether the minimum estimation error given by Eq. (2) can be practically achieved, depends on the actual measurement performed on the BTC light. In this protocol, the source output light first probes the unknown sample acquiring the phase shift  $\varphi$  and it is then superposed with the emission field of a strong local oscillator, using a low reflectivity beam splitter (LRBS) [see Fig. 1(d)]. We compute the estimation error  $\delta\varphi$  for this protocol and show, that it saturates the QCRB in the stationary regime, but cannot harness the enhancement in the time crystal regime anticipated by the QFI. This setup allows for the measurement of the homodyne current extracted at the indicated output port [8, 69]

$$J_{\beta}(t) = \sqrt{\kappa} \langle \hat{S}_{\beta}(t) \rangle_{\text{H}} + \frac{dW}{dt}, \quad (5)$$

where  $\hat{S}_{\beta} = \hat{S}_{-} e^{i(\beta-\varphi)} + \hat{S}_{+} e^{-i(\beta-\varphi)}$  is a general quadrature, parametrized by the homodyne phase  $\beta$  defined by the chosen LRBS, and  $dW/dt$  the derivative of a Wiener process. The subscript H indicates expectation values taken with respect to the conditional state of the homodyne unravelling [8, 69].

We assume ideal monitoring of the homodyne current over a long measurement time  $T$ , and neglect any additional loss channels. Thus,  $\varphi$  can be estimated by measuring the long-time average of the homodyne current,  $J_T = (1/T) \int_0^T J_{\beta}(t) dt$ . Its average value reads  $\mathbb{E}[J_T] = (\sqrt{\kappa}/T) \int_0^T \langle \hat{S}_{\beta}(t) \rangle dt$  with  $\mathbb{E}[\bullet]$  the average over trajectories and  $\langle \mathcal{O}(t) \rangle = \text{Tr}[\mathcal{O}\rho(t)]$  the unconditional expectation value. For the estimation error, the error propagation formula holds [42]

$$\delta\varphi = \sqrt{\mathbb{E}[J_T^2] - \mathbb{E}[J_T]^2} \left| \frac{\partial \mathbb{E}[J_T]}{\partial \varphi} \right|^{-1}, \quad (6)$$

which is lower bounded by the QCRB Eq. (2). In the long-time limit, the time averaged homodyne current approaches its ensemble mean  $\lim_{T \rightarrow \infty} J_T = \sqrt{\kappa} \langle \hat{S}_{\beta} \rangle_{\text{ss}}$  [69]. Far away from critical points, large deviations theory yields a behavior of the standard deviation as  $\sqrt{\mathbb{E}[J_T^2] - \mathbb{E}[J_T]^2} \sim \sigma_{J_T}/\sqrt{T}$  [71], with the time independent rescaled standard deviation  $\sigma_{J_T}$ . This implies a behavior of the estimation error in the long-time limit as  $\delta\varphi \sim \overline{\delta\varphi}/\sqrt{T}$ , with the long-time rescaled estimation error  $\overline{\delta\varphi}$ . An HP approach in the stationary regime yields [66]

$$\overline{\delta\varphi} \approx \frac{\sqrt{\kappa}}{2\omega |\cos(\varphi - \beta)|}. \quad (7)$$

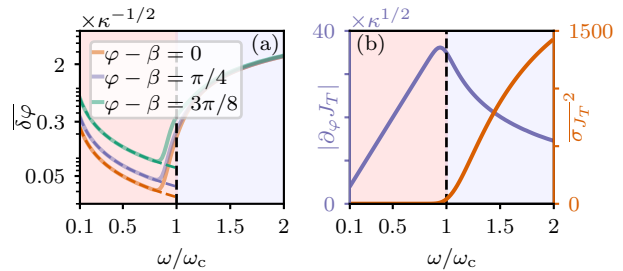


FIG. 2. **Estimation error using the average homodyne current protocol.** (a) Time rescaled long-time estimation error  $\delta\varphi$  for the homodyne protocol as a function of the Rabi frequency  $\omega$ , for  $N = 40$  and different values of  $\varphi - \beta$ . The dashed lines represent the respective Holstein-Primakoff (HP) approximated curves. (b) Derivative of the long-time averaged homodyne current  $|\partial_{\varphi} J_T|$  and its variance  $\sigma_{J_T}^2$  as a function of the Rabi frequency  $\omega/\omega_c$ , for  $N = 40$  and  $\varphi - \beta = 0$ .

This agrees with the numerical results presented in Fig. 2(a) deep in the stationary regime, and saturates the QCRB for  $\varphi - \beta = 0$ . For  $\varphi - \beta = 0$ , the quadrature  $\hat{S}_{\beta} = \hat{S}_{\text{x}}$ , for which the long-time average vanishes,  $\langle \hat{S}_{\text{x}} \rangle_{\text{ss}} = 0$  [8]. This can be interpreted as a signature in the measurement data when tuning through the parameter  $\beta$  [see Fig. 1(e)]. We further find, that in the vicinity of the critical Rabi frequency, the estimation error increases to a higher level in the time crystal regime than the minimum observed in the stationary regime. The increment of the estimation error in the time crystal regime is rooted in the larger variance of the time averaged homodyne current and a smaller value of the derivative with respect to  $\varphi$  displayed in this regime [see Fig. 2(b)].

*Perfect absorber protocol.*— The average homodyne current protocol is not capable of exploiting the intricate time-correlations of the BTC light. This demands for a detection scheme that can extract the information encoded in the phase shifted output field in the time crystal regime. Next, we show that this can be achieved by constructing a perfect absorber for the BTC light [63, 64, 72]. In fact, this absorber is a replica BTC, acting as a 'decoder' for the information inscribed on the phase shifted light [see Fig. 1(b)].

In this protocol, the light emitted by the source BTC acquires a phase  $\varphi$  and is then unidirectionally guided into the decoder system. By applying an auxiliary tunable phase shift  $\varphi'$  to the decoder output, the optical phase  $\varphi$  can be estimated by means of an intensity measurement of the decoder output [see Fig. 1(c)]. The evolution of the emerging cascaded system shown in Fig. 1(b) is described by the master equation [42, 63, 72]

$$\partial_t \rho = -i[\omega(\hat{S}_{\text{x}}^{\text{S}} + \hat{S}_{\text{x}}^{\text{D}}) + \hat{H}_{\text{casc}}, \rho] + \kappa \mathcal{D}[\hat{L}_{\text{casc}}] \rho, \quad (8)$$

with  $\hat{H}_{\text{casc}} = -(i\kappa/2)(e^{-i\Delta\varphi} \hat{S}_{+}^{\text{D}} \hat{S}_{-}^{\text{S}} - e^{i\Delta\varphi} \hat{S}_{+}^{\text{S}} \hat{S}_{-}^{\text{D}})$ ,  $\hat{L}_{\text{casc}} = e^{-i\Delta\varphi} \hat{S}_{-}^{\text{S}} + \hat{S}_{-}^{\text{D}}$ , the phase difference  $\Delta\varphi = \varphi - \varphi'$ , and the superscript S (D) labels the collective operators of the source (decoder). The cascaded system described

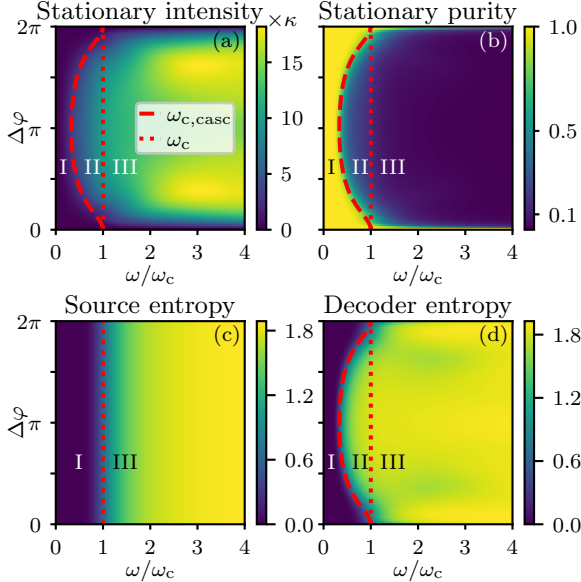


**FIG. 3. Stationary properties of the cascaded system.**  $N = 6$  for all panels. (a) Time averaged intensity in the stationary state as a function of Rabi frequency  $\omega$  and phase difference  $\Delta\varphi$ . (b) Purity of the stationary state as a function of Rabi frequency  $\omega$  and phase difference  $\Delta\varphi$ . (c)-(d) Von Neumann entropy  $S_{VN}$  reduced to the source (c) and to the decoder (d) in the stationary state. For (a), (b) and (d), the red dashed line indicates the cascaded mean field transition line  $\omega_{c,casc}$  from the stationary regime (I) to an intermediate regime, where only the decoder is in a time crystal regime (II). For (a)-(d), the red dotted line corresponds to the single system transition line  $\omega_c$  and marks the transition to a regime where both source and decoder display time crystal behavior (III).

by Eq. (8) features a pure dark state at  $\Delta\varphi = 0$  as derived in Ref. [42], which renders the decoder system a perfect absorber for this choice of parameters [72]. The occurrence of the dark state is independent of the Rabi frequency  $\omega$ , which is highlighted in Fig. 3(a). For general values of  $\Delta\varphi$ , the behavior with respect to the Rabi frequency can be partitioned in three different regimes, with the critical frequency  $\omega_c$  and the cascaded critical frequency  $\omega_{c,casc} = \omega_c / \sqrt{5 - 4 \cos(\Delta\varphi)}$  separating them. For  $\omega < \omega_{c,casc}$ , both source and decoder are in the single system stationary regime (regime I in Fig. 3). For  $\omega_{c,casc} \leq \omega < \omega_c$ , the decoder first transitions to a time crystal regime, with its observables showing persistent temporal oscillations in the thermodynamic limit (II) [66]. For  $\omega \geq \omega_c$ , both the source and the decoder are in a time crystal regime (III). This behavior is reflected by the von Neuman entropy  $S_{VN} = -\text{Tr}[\rho_{ss}^i \ln \rho_{ss}^i]$  of the stationary state reduced to the source ( $i = S$ ) and the decoder ( $i = D$ ). For the source, a transition from a pure to a mixed stationary state can be observed at  $\omega = \omega_c$ , whereas for the decoder this transition occurs at  $\omega = \omega_{c,casc}$ .

We study the performance of the perfect absorber pro-

ocol, considering a setup in which we estimate  $\varphi$  using the time averaged intensity  $I_T = (1/T) \int_0^T dN(t)$  of the cascaded system.  $dN(t)$  is a random variable taking the values 1 if a photon is detected at time  $t$  and 0 otherwise [69]. Its average value over all possible measurement trajectories is  $\mathbb{E}[dN(t)] = \kappa dt \langle \hat{L}_{\text{casc}}^\dagger \hat{L}_{\text{casc}}(t) \rangle$ , with an infinitesimal time step  $dt$  [69]. The estimation error for such measurement is given by the error propagation formula Eq. (6) with  $J_T$  replaced by  $I_T$  [42]. For long measurement times, the time averaged intensity approaches its mean value  $\lim_{T \rightarrow \infty} I_T = \kappa \langle \hat{L}_{\text{casc}}^\dagger \hat{L}_{\text{casc}} \rangle_{\text{ss}}$  [69], and far away from critical points  $\sqrt{\mathbb{E}[I_T^2] - \mathbb{E}[I_T]^2} \sim \overline{\sigma_{I_T}} / \sqrt{T}$ , with the time rescaled standard deviation  $\overline{\sigma_{I_T}}$  [73, 74]. Ultimately this leads to a scaling of the estimation error in the long-time limit as  $\delta\varphi \sim \overline{\delta\varphi} / \sqrt{T}$ , with the long-time rescaled estimation error  $\overline{\delta\varphi} = \overline{\sigma_{I_T}} / |\partial_\varphi I_T|$ .

By using an HP approach we determine the estimation error in the cascaded stationary regime [66]

$$\overline{\delta\varphi} \approx \sqrt{\frac{\kappa(1 - \cos(\Delta\varphi))}{2\omega^2 \sin^2(\Delta\varphi)}}. \quad (9)$$

This saturates the QCRB for  $\Delta\varphi \rightarrow 0$  and is numerically verified in Fig. 4(a). Alternatively, in the SM [66], we also show the optimality of the perfect absorber protocol in the stationary regime by using the techniques developed in Ref. [63]. In the time crystal regime and close to the perfect absorber condition  $\Delta\varphi = 0$ , we observe lower values of the estimation error than in the stationary regime. This has a twofold reason: On the one hand,  $\overline{\sigma_{I_T}}$  decreases with  $\Delta\varphi$  in the vicinity of  $\Delta\varphi = 0$ , leading to lower estimation errors. On the other hand,  $|\partial_\varphi I_T|$  displays a maximum, which moves closer to  $\Delta\varphi = 0$  with increasing system size, leading to smaller estimation errors at this maximum [see Fig. 4(c)]. As a function of system size, we find beyond Heisenberg scaling proportional to  $\overline{\delta\varphi} \propto N^{-\alpha}$  with  $\alpha = 1.222 \pm 0.018$  for  $\Delta\varphi = 0.005$ , and  $\alpha = 1.04 \pm 0.04$  for  $\Delta\varphi = 0.01$ , both for a Rabi frequency of  $\omega/\omega_c = 4$  [see Fig. 4(b)].

*Conclusions and Outlook.*— We showed that a BTC can be used as a light source for collectively enhanced sensing of an optical phase shift encoded by an unknown sample. In the time crystal regime, we found that the QFI for sensing optical phases scales as  $N^4$  in the size  $N$  of the BTC, surpassing Heisenberg scaling of  $N^2$  in the stationary regime. We constructed a detector based on the idea of building a perfect absorber and demonstrated, that it is capable of extracting the correlations in the phase shifted BTC light and thus allows beyond Heisenberg scaling of the phase estimation error.

The largely analytically tractable BTC serves as a convenient theoretical platform for demonstrating the concept behind quantum enhanced parameter estimation using collective quantum many-body systems as light sources. However, further work is necessary to bridge the gap between this model and practical experimental

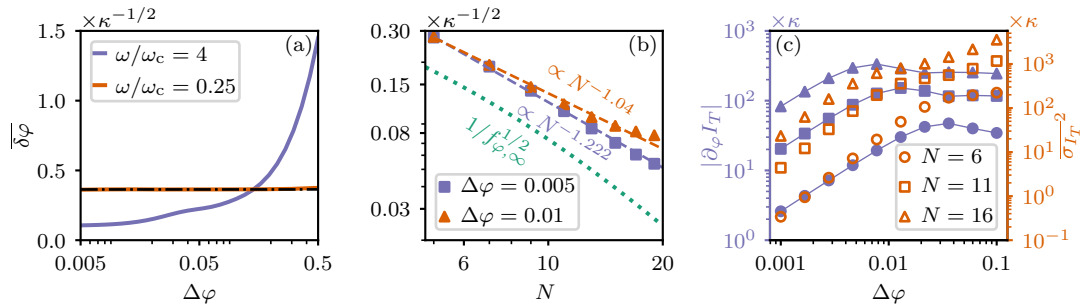


FIG. 4. **Estimation error using the perfect absorber protocol.** (a) Time rescaled long-time estimation error as a function of phase difference  $\Delta\varphi$ , for  $\omega/\omega_c = 4$  in the cascaded time crystal regime (III) and  $\omega/\omega_c = 0.25$  in the cascaded stationary regime (I), and system size  $N = 11$ . The black dashed-dotted line is the HP approximated result for  $\omega/\omega_c = 0.25$ . (b) Estimation error as a function of system size for different values of  $\Delta\varphi$ , and  $\omega/\omega_c = 4$  in the cascaded time crystal regime (III). The green dotted line indicates the limiting values given by the quantum Fisher information (QFI) rate in the limit of  $\omega/\omega_c \rightarrow \infty$ . Fitting a power law  $\bar{\delta}\varphi = bN^{-\alpha}$  through the presented data points yields the scaling exponents  $\alpha = 1.222 \pm 0.018$  for  $\Delta\varphi = 0.005$  and  $\alpha = 1.04 \pm 0.04$  for  $\Delta\varphi = 0.01$ . (c) Absolute derivative and variance of the time averaged intensity as a function of the phase difference  $\Delta\varphi$ , for different system sizes and fixed value  $\omega/\omega_c = 4$ , in the cascaded time crystal regime.

implementations. Future research will need to incorporate factors such as finite detection efficiencies [45], as well as the effects of other loss channels like local decay [43], which can influence measurement precision. Additionally, it will be important to investigate whether more experimentally feasible measurement schemes, such as interferometric protocols capable of detecting multi-time correlations [43], can effectively process the phase shifted BTC light and achieve enhanced precision. In the longer term, an intriguing and challenging direction will be to explore whether the observed quantum enhancements persist in light emitted from other types of time crystals, particularly in systems involving particles with finite-range interactions and non-collective dissipation [75, 76].

Code and data in support of the findings of this paper are available on GitHub [77].

**Acknowledgements.**— We acknowledge the use of the QuTiP library [78–80]. We acknowledge support from the Deutsche Forschungsgemeinschaft (DFG, German Research Foundation) through the Walter Benjamin programme, Grant No. 519847240 and the Research Unit FOR 5413/1. This work was supported by the QuantERA II programme (project CoQuaDis, DFG Grant No. 532763411) that has received funding from the EU H2020 research and innovation programme under GA No. 101017733. This work is also supported by the ERC grant OPEN-2QS (Grant No. 101164443, <https://doi.org/10.3030/101164443>).

ligo gravitational wave detector by using squeezed states of light, *Nature Photon.* **7**, 613 (2013).

- [3] D. Meiser, J. Ye, D. R. Carlson, and M. J. Holland, Prospects for a millihertz-linewidth laser, *Phys. Rev. Lett.* **102**, 163601 (2009).
- [4] D. Meiser and M. J. Holland, Intensity fluctuations in steady-state superradiance, *Phys. Rev. A* **81**, 063827 (2010).
- [5] M. Xu, D. A. Tieri, E. C. Fine, J. K. Thompson, and M. J. Holland, Synchronization of two ensembles of atoms, *Phys. Rev. Lett.* **113**, 154101 (2014).
- [6] M. Xu and M. J. Holland, Conditional ramsey spectroscopy with synchronized atoms, *Phys. Rev. Lett.* **114**, 103601 (2015).
- [7] F. Iemini, A. Russomanno, J. Keeling, M. Schirò, M. Dalmonte, and R. Fazio, Boundary time crystals, *Phys. Rev. Lett.* **121**, 035301 (2018).
- [8] A. Cabot, L. S. Muhle, F. Carollo, and I. Lesanovsky, Quantum trajectories of dissipative time crystals, *Phys. Rev. A* **108**, L041303 (2023).
- [9] H. Kefler, P. Kongkhambut, C. Georges, L. Mathey, J. G. Cosme, and A. Hemmerich, Observation of a dissipative time crystal, *Phys. Rev. Lett.* **127**, 043602 (2021).
- [10] K. Sacha and J. Zakrzewski, Time crystals: a review, *Rep. Prog. Phys.* **81**, 016401 (2017).
- [11] D. V. Else, C. Monroe, C. Nayak, and N. Y. Yao, Discrete time crystals, *Annu. Rev. Condens. Matter Phys.* **11**, 467 (2020).
- [12] M. P. Zaletel, M. Lukin, C. Monroe, C. Nayak, F. Wilczek, and N. Y. Yao, Colloquium: Quantum and classical discrete time crystals, *Rev. Mod. Phys.* **95**, 031001 (2023).
- [13] H. J. Carmichael, Analytical and numerical results for the steady state in cooperative resonance fluorescence, *J. Phys. B: Atom. Mol. Phys.* **13**, 3551 (1980).
- [14] D. V. Else, B. Bauer, and C. Nayak, Floquet time crystals, *Phys. Rev. Lett.* **117**, 090402 (2016).
- [15] V. Khemani, A. Lazarides, R. Moessner, and S. L. Sondhi, Phase structure of driven quantum systems, *Phys. Rev. Lett.* **116**, 250401 (2016).
- [16] Z. Gong, R. Hamazaki, and M. Ueda, Discrete time-crystalline order in cavity and circuit qed systems, *Phys. Rev. Lett.* **120**, 040404 (2018).

[17] N. Y. Yao, A. C. Potter, I.-D. Potirniche, and A. Vishwanath, Discrete time crystals: Rigidity, criticality, and realizations, *Phys. Rev. Lett.* **118**, 030401 (2017).

[18] R. R. W. Wang, B. Xing, G. G. Carlo, and D. Poletti, Period doubling in period-one steady states, *Phys. Rev. E* **97**, 020202 (2018).

[19] F. M. Gambetta, F. Carollo, M. Marcuzzi, J. P. Garrahan, and I. Lesanovsky, Discrete time crystals in the absence of manifest symmetries or disorder in open quantum systems, *Phys. Rev. Lett.* **122**, 015701 (2019).

[20] A. Lazarides, S. Roy, F. Piazza, and R. Moessner, Time crystallinity in dissipative floquet systems, *Phys. Rev. Res.* **2**, 022002 (2020).

[21] A. Riera-Campeny, M. Moreno-Cardoner, and A. Sanpera, Time crystallinity in open quantum systems, *Quantum* **4**, 270 (2020).

[22] B. Zhu, J. Marino, N. Y. Yao, M. D. Lukin, and E. A. Demler, Dicke time crystals in driven-dissipative quantum many-body systems, *New J. Phys.* **21**, 073028 (2019).

[23] K. Chinzei and T. N. Ikeda, Time crystals protected by floquet dynamical symmetry in hubbard models, *Phys. Rev. Lett.* **125**, 060601 (2020).

[24] R. J. L. Tuquero, J. Skulte, L. Mathey, and J. G. Cosme, Dissipative time crystal in an atom-cavity system: Influence of trap and competing interactions, *Phys. Rev. A* **105**, 043311 (2022).

[25] S. Sarkar and Y. Dubi, Signatures of discrete time-crystallinity in transport through an open fermionic chain, *Commun. Phys.* **5**, 155 (2022).

[26] A. Cabot, F. Carollo, and I. Lesanovsky, Metastable discrete time-crystal resonances in a dissipative central spin system, *Phys. Rev. B* **106**, 134311 (2022).

[27] F. Carollo and I. Lesanovsky, Exact solution of a boundary time-crystal phase transition: Time-translation symmetry breaking and non-markovian dynamics of correlations, *Phys. Rev. A* **105**, L040202 (2022).

[28] K. Tucker, B. Zhu, R. J. Lewis-Swan, J. Marino, F. Jimenez, J. G. Restrepo, and A. M. Rey, Shattered time: can a dissipative time crystal survive many-body correlations?, *New J. Phys.* **20**, 123003 (2018).

[29] C. Lledó and M. H. Szymańska, A dissipative time crystal with or without  $z2$  symmetry breaking, *New J. Phys.* **22**, 075002 (2020).

[30] B. Buča and D. Jaksch, Dissipation induced nonstationarity in a quantum gas, *Phys. Rev. Lett.* **123**, 260401 (2019).

[31] B. Buča, J. Tindall, and D. Jaksch, Non-stationary coherent quantum many-body dynamics through dissipation, *Nat. Commun.* **10**, 1730 (2019).

[32] C. Booker, B. Buča, and D. Jaksch, Non-stationarity and dissipative time crystals: spectral properties and finite-size effects, *New J. Phys.* **22**, 085007 (2020).

[33] G. Buonaiuto, F. Carollo, B. Olmos, and I. Lesanovsky, Dynamical phases and quantum correlations in an emitter-waveguide system with feedback, *Phys. Rev. Lett.* **127**, 133601 (2021).

[34] L. F. d. Prazeres, L. d. S. Souza, and F. Iemini, Boundary time crystals in collective  $d$ -level systems, *Phys. Rev. B* **103**, 184308 (2021).

[35] G. Piccitto, M. Wauters, F. Nori, and N. Shammah, Symmetries and conserved quantities of boundary time crystals in generalized spin models, *Phys. Rev. B* **104**, 014307 (2021).

[36] A. C. Lourenço, L. F. d. Prazeres, T. O. Maciel, F. Iemini, and E. I. Duzzioni, Genuine multipartite correlations in a boundary time crystal, *Phys. Rev. B* **105**, 134422 (2022).

[37] M. Hajdušek, P. Solanki, R. Fazio, and S. Vinjanampathy, Seeding crystallization in time, *Phys. Rev. Lett.* **128**, 080603 (2022).

[38] M. Krishna, P. Solanki, M. Hajdušek, and S. Vinjanampathy, Measurement-induced continuous time crystals, *Phys. Rev. Lett.* **130**, 150401 (2023).

[39] R. Mattes, I. Lesanovsky, and F. Carollo, Entangled time-crystal phase in an open quantum light-matter system, *Phys. Rev. A* **108**, 062216 (2023).

[40] G. Ferioli, A. Glicenstein, I. Ferrier-Barbut, and A. Browaeys, A non-equilibrium superradiant phase transition in free space, *Nat. Phys.* **19**, 1345 (2023).

[41] V. Montenegro, M. G. Genoni, A. Bayat, and M. G-A Paris, Quantum metrology with boundary time crystals, *Commun. Phys.* **6**, 304 (2023).

[42] A. Cabot, F. Carollo, and I. Lesanovsky, Continuous sensing and parameter estimation with the boundary time crystal, *Phys. Rev. Lett.* **132**, 050801 (2024).

[43] A. Cabot, F. Carollo, and I. Lesanovsky, Quantum enhanced parameter estimation with monitored quantum nonequilibrium systems using inefficient photo detection (2025), [arXiv:2503.21753 \[quant-ph\]](https://arxiv.org/abs/2503.21753).

[44] R. Mattes, A. Cabot, F. Carollo, and I. Lesanovsky, Designing open spin-boson models for enabling quantum enhanced sensing through classical measurements (2025), [arXiv:2505.08756 \[quant-ph\]](https://arxiv.org/abs/2505.08756).

[45] E. O'Connor, V. Montenegro, F. Albarelli, M. G. A. Paris, A. Bayat, and M. G. Genoni, Quantum-enhanced parameter estimation in continuously monitored boundary time crystals (2025), [arXiv:2508.15448 \[quant-ph\]](https://arxiv.org/abs/2508.15448).

[46] D. Gribben, A. Sanpera, R. Fazio, J. Marino, and F. Iemini, Boundary time crystals as ac sensors: Enhancements and constraints, *SciPost Phys.* **18**, 100 (2025).

[47] S. Gammelmark and K. Mølmer, Fisher information and the quantum cramér-rao sensitivity limit of continuous measurements, *Phys. Rev. Lett.* **112**, 170401 (2014).

[48] K. Macieszczak, M. Guță, I. Lesanovsky, and J. P. Garrahan, Dynamical phase transitions as a resource for quantum enhanced metrology, *Phys. Rev. A* **93**, 022103 (2016).

[49] T. Ilias, D. Yang, S. F. Huelga, and M. B. Plenio, Criticality-enhanced quantum sensing via continuous measurement, *PRX Quantum* **3**, 010354 (2022).

[50] J. Gambetta and H. M. Wiseman, State and dynamical parameter estimation for open quantum systems, *Phys. Rev. A* **64**, 042105 (2001).

[51] C. Catana, M. van Horssen, and M. Guta, Asymptotic inference in system identification for the atom maser, *Phil. Trans. R. Soc. A* (2012).

[52] S. Gammelmark and K. Mølmer, Bayesian parameter inference from continuously monitored quantum systems, *Phys. Rev. A* **87**, 032115 (2013).

[53] A. H. Kiilerich and K. Mølmer, Estimation of atomic interaction parameters by photon counting, *Phys. Rev. A* **89**, 052110 (2014).

[54] F. Albarelli, M. A. C. Rossi, M. G. A. Paris, and M. G. Genoni, Ultimate limits for quantum magnetometry via time-continuous measurements, *New J. Phys.* **19**, 123011 (2017).

[55] F. Albarelli, M. A. C. Rossi, D. Tamascelli, and M. G.

Genoni, Restoring Heisenberg scaling in noisy quantum metrology by monitoring the environment, *Quantum* **2**, 110 (2018).

[56] A. Shankar, G. P. Greve, B. Wu, J. K. Thompson, and M. Holland, Continuous real-time tracking of a quantum phase below the standard quantum limit, *Phys. Rev. Lett.* **122**, 233602 (2019).

[57] F. Albarelli, M. A. C. Rossi, and M. G. Genoni, Quantum frequency estimation with conditional states of continuously monitored independent dephasing channels, *Int. J. Quantum. Inform.* **18**, 1941013 (2020).

[58] M. A. C. Rossi, F. Albarelli, D. Tamascelli, and M. G. Genoni, Noisy quantum metrology enhanced by continuous nondemolition measurement, *Phys. Rev. Lett.* **125**, 200505 (2020).

[59] J. Amorós-Binefa and J. Kołodyński, Noisy atomic magnetometry in real time, *New J. Phys.* **23**, 123030 (2021).

[60] H. I. Nurdin and M. Gută, Parameter estimation and system identification for continuously-observed quantum systems, *Annu. Rev. Control* **54**, 295 (2022).

[61] M. Radaelli, J. A. Smiga, G. T. Landi, and F. C. Binder, Parameter estimation for quantum jump unravelling (2024), arXiv:2402.06556 [quant-ph].

[62] J. Amorós-Binefa and J. Kołodyński, Noisy atomic magnetometry with kalman filtering and measurement-based feedback, *PRX Quantum* **6**, 030331 (2025).

[63] D. Yang, S. F. Huelga, and M. B. Plenio, Efficient information retrieval for sensing via continuous measurement, *Phys. Rev. X* **13**, 031012 (2023).

[64] A. Godley and M. Gută, Adaptive measurement filter: efficient strategy for optimal estimation of quantum Markov chains, *Quantum* **7**, 973 (2023).

[65] C. W. Gardiner and P. Zoller, *Quantum Noise* (Springer-Verlag, Berlin, 2004).

[66] See Supplemental Material for details on the representation of the system and environment state, the analytical and numerical calculations of the QFI and estimation error, and on the mean-field dynamics of the sensor-decoder setup.

[67] H. Cramér, *Mathematical Methods of Statistics* (Princeton University Press, Princeton, 1946).

[68] S. L. Braunstein and C. M. Caves, Statistical distance and the geometry of quantum states, *Phys. Rev. Lett.* **72**, 3439 (1994).

[69] H. M. Wiseman and G. J. Milburn, *Quantum Measurement and Control* (Cambridge University Press, Cambridge, 2009).

[70] D. Nemeth, A. Principi, and A. Nazir, Solving boundary time crystals via the superspin method (2025), arXiv:2507.06998 [quant-ph].

[71] J. M. Hickey, S. Genway, I. Lesanovsky, and J. P. Garrahan, Thermodynamics of quadrature trajectories in open quantum systems, *Phys. Rev. A* **86**, 063824 (2012).

[72] K. Stannigel, P. Rabl, and P. Zoller, Driven-dissipative preparation of entangled states in cascaded quantum-optical networks, *New J. Phys.* **14**, 063014 (2012).

[73] J. P. Garrahan and I. Lesanovsky, Thermodynamics of quantum jump trajectories, *Phys. Rev. Lett.* **104**, 160601 (2010).

[74] F. Carollo, J. P. Garrahan, I. Lesanovsky, and C. Pérez-Espigares, Making rare events typical in markovian open quantum systems, *Phys. Rev. A* **98**, 010103 (2018).

[75] F. Russo and T. Pohl, Quantum dissipative continuous time crystals, *Phys. Rev. Lett.* **135**, 110404 (2025).

[76] Z. Wang, R. Gao, X. Wu, B. Buča, K. Mølmer, L. You, and F. Yang, Boundary time crystals induced by local dissipation and long-range interactions (2025), 2503.20761 [quant-ph].

[77] M. Jirasek, I. Lesanovsky, and A. Cabot, Code and data of "the boundary time crystal as a source of light for quantum enhanced sensing beyond the heisenberg limit" (2025), <https://github.com/malikjirasek/The-Boundary-Time-Crystal-as-a-source-of-light-for-quantum-enhanced-sensing-beyond-the-Heisenberg>.

[78] J. Johansson, P. Nation, and F. Nori, Qutip: An open-source python framework for the dynamics of open quantum systems, *Comput. Phys. Commun.* **183**, 1760 (2012).

[79] J. Johansson, P. Nation, and F. Nori, Qutip 2: A python framework for the dynamics of open quantum systems, *Comput. Phys. Commun.* **184**, 1234 (2013).

[80] N. Lambert, E. Giguère, P. Menczel, B. Li, P. Hopf, G. Suárez, M. Gali, J. Lishman, R. Gadhvi, R. Agarwal, A. Galicia, N. Shammah, P. Nation, J. R. Johansson, S. Ahmed, S. Cross, A. Pitchford, and F. Nori, Qutip 5: The quantum toolbox in python (2024), 2412.04705.

[81] F. Verstraete and J. I. Cirac, Continuous matrix product states for quantum fields, *Phys. Rev. Lett.* **104**, 190405 (2010).

[82] J. Haegeman, J. I. Cirac, T. J. Osborne, and F. Verstraete, Calculus of continuous matrix product states, *Phys. Rev. B* **88**, 085118 (2013).

[83] R. Puri and S. Lawande, Exact steady-state density operator for a collective atomic system in an external field, *Phys. Lett. A* **72**, 200 (1979).

[84] J. Hannukainen and J. Larson, Dissipation-driven quantum phase transitions and symmetry breaking, *Phys. Rev. A* **98**, 042113 (2018).

[85] P. Zoller, M. Marte, and D. F. Walls, Quantum jumps in atomic systems, *Phys. Rev. A* **35**, 198 (1987).

[86] F. Ciccarello, S. Lorenzo, V. Giovannetti, and G. M. Palma, Quantum collision models: Open system dynamics from repeated interactions, *Phys. Rep.* **954**, 1 (2022).

[87] L. Pezzè, M. A. Ciampini, N. Spagnolo, P. C. Humphreys, A. Datta, I. A. Walmsley, M. Barbieri, F. Sciarrino, and A. Smerzi, Optimal measurements for simultaneous quantum estimation of multiple phases, *Phys. Rev. Lett.* **119**, 130504 (2017).

[88] J. Liu, H. Yuan, X.-M. Lu, and X. Wang, Quantum fisher information matrix and multiparameter estimation, *J. Phys. A: Math. Theor.* **53**, 023001 (2019).

[89] L. Pezzè and A. Smerzi, Quantum Theory of Phase Estimation, in *Proceedings of the International School of Physics "Enrico Fermi"*, Vol. 188 (IOS Press, Amsterdam, 2014).

[90] F. Benatti, F. Carollo, R. Floreanini, and H. Narnhofer, Quantum spin chain dissipative mean-field dynamics, *J. Phys. A: Math. Theor.* **51**, 325001 (2018).

[91] O. E. Lanford and D. Ruelle, Observables at infinity and states with short range correlations in statistical mechanics, *Commun. Math. Phys.* **13**, 194 (1969).

## SUPPLEMENTAL MATERIAL

### Quantum Sensing beyond the Heisenberg Limit with the Boundary Time Crystal

Malik Jirasek<sup>1</sup>, Igor Lesanovsky<sup>1,2</sup>, and Albert Cabot<sup>1</sup>

<sup>1</sup>*Institut für Theoretische Physik, Universität Tübingen,  
Auf der Morgenstelle 14, 72076 Tübingen, Germany*

<sup>2</sup>*School of Physics and Astronomy and Centre for the Mathematics and Theoretical Physics of Quantum Non-Equilibrium Systems, The University of Nottingham, Nottingham, NG7 2RD, United Kingdom*

#### QFI WITH MPS DESCRIPTION

We consider the estimation of an optical phase shift  $\varphi$  imprinted on the photons emitted by a quantum system as described by Eq. (1). This phase shift is described by the transformation of the jump operator  $\hat{L} \rightarrow \hat{L}e^{-i\varphi}$  [48]. The estimation error of any measurement of a classical parameter imprinted on the state of a quantum system is lower bounded by the QCRB [67, 69]

$$\text{Var}[\hat{\varphi}]_{\varphi_0} \geq 1/F_{\varphi}(\varphi_0, T), \quad (\text{S1})$$

where  $\text{Var}[\hat{\varphi}]_{\varphi_0}$  is the variance of the estimator  $\hat{\varphi}$  for the physical parameter  $\varphi$  evaluated at a realization  $\varphi_0$ .  $F_{\varphi}(\varphi_0, T)$  is the QFI associated to the parameter  $\varphi$  at measurement time  $T$  evaluated at  $\varphi_0$ . In the following, we will consider  $\delta\varphi = \sqrt{\text{Var}[\hat{\varphi}]_{\varphi_0}}$  as a measure for the estimation error for the parameter  $\varphi$ . The QFI can be computed, using the symmetric logarithmic derivative (SLD)  $D$  with [48]

$$\partial_{\varphi}\rho = \frac{1}{2} (D\rho + \rho D), \quad (\text{S2})$$

where  $\rho$  is the global density matrix. The QFI is given in terms of the SLD as [48]

$$F_{\varphi}(\varphi, T) = \text{Var}[D]_{\varphi}, \quad (\text{S3})$$

meaning that it only depends on the global quantum state  $\rho_{\varphi}$  and the form of the SLD. Since the QFI is optimized over all possible measurements, it does not depend on or specifies measurements [69]. For a pure quantum state  $\rho_{\varphi} = |\psi_{\varphi}\rangle\langle\psi_{\varphi}|$ , the QFI takes the more simple form [47, 48]

$$\begin{aligned} F_{\varphi}(\varphi, T) &= 4 (\langle\psi'_{\varphi}|\psi'_{\varphi}\rangle - |\langle\psi'_{\varphi}|\psi_{\varphi}\rangle|^2) \\ &= 4\partial_{\varphi_1}\partial_{\varphi_2} \ln \langle\psi_{\varphi_1}|\psi_{\varphi_2}\rangle, \end{aligned} \quad (\text{S4})$$

where  $|\psi'_{\varphi}\rangle = \partial_{\varphi}|\psi_{\varphi}\rangle$  is the derivative of the state. In the case of a quantum system described by Eq. (1), the global system and environment state at time  $T$  can be approximated by the matrix product state [43, 47]

$$|\psi_{\varphi}\rangle = \sum_{i_1, \dots, i_n=0}^1 K_{i_n} \cdots K_{i_1} |\chi_S\rangle \otimes |i_1, \dots, i_n\rangle, \quad (\text{S5})$$

where we have discretized time into  $n$  steps of size  $\delta t$ , and introduced the Kraus operators  $K_0 = 1 - i\delta t\hat{H} - \kappa\delta t\hat{L}^{\dagger}\hat{L}/2$  and  $K_1 = \sqrt{\kappa\delta t}\hat{L}e^{-i\varphi}$ . The choice of the Kraus operators given here assumes an ideal photoncounting picture of the emission statistics. A similar description can be found, assuming ideal homodyne detection [44]. In the limit of infinitesimal time steps, the MPS Eq. (S5) becomes a continuous matrix product state (cMPS) and one recovers the dynamics of Eq. (S9) [48, 81, 82].  $|\chi_S\rangle$  is the initial system state and  $|i_1, \dots, i_n\rangle$  captures the time record of detected emissions into a bosonic environment.

Using the MPS description and the second equation of Eq. (S4), the QFI rate in the long-time limit reads

$$f_{\varphi} := \lim_{T \rightarrow \infty} \frac{F_{\varphi}(\varphi, T)}{T} = 4\partial_{\varphi_1}\partial_{\varphi_2}\lambda_0(\Delta\varphi)|_{\Delta\varphi=0}, \quad (\text{S6})$$

where  $\lambda_0(\Delta\varphi)$  is the eigenvalue with largest real part of the deformed master equation

$$\partial_t \rho = \mathcal{L}[\rho] + \kappa (e^{-i\Delta\varphi} - 1) \hat{L} \rho \hat{L}^\dagger, \quad (\text{S7})$$

with  $\mathcal{L}$  the Lindbladian describing evolution according to Eq. (1).

Alternatively, we determine the QFI by computing the inner products in the first line of Eq. (S4) [47]. This yields

$$\begin{aligned} \langle \psi_\varphi | \psi'_\varphi \rangle &= \sum_{j=1}^n \text{Tr} \left[ \rho(t_{j-1}) (-i\kappa\delta t) \hat{L}^\dagger \hat{L} \right] \xrightarrow{\delta t \rightarrow 0} -i\kappa \int_0^T dt \text{Tr} \left[ \rho(t) \hat{L}^\dagger \hat{L} \right] \\ \langle \psi'_\varphi | \psi'_\varphi \rangle &= \sum_{j=1}^n \text{Tr} \left[ \rho(t_{j-1}) \kappa \delta t \hat{L}^\dagger \hat{L} \right] + 2 \sum_{j>k=1}^n \text{Tr} \left[ \kappa^2 \delta t^2 \hat{L}^\dagger \hat{L} (\hat{L} \rho(t_{k-1}) \hat{L}^\dagger) (t_{j-1} - t_{k+1}) \right] \\ &\xrightarrow{\delta t \rightarrow 0} \int_0^T dt \text{Tr} \left[ \rho(t) \hat{L}^\dagger \hat{L} \right] + 2\kappa^2 \int_0^T dt \int_0^{T-t} d\tau \underbrace{\text{Tr} \left[ \hat{L}^\dagger \hat{L} e^{\mathcal{L}\tau} (\hat{L} \rho(t) \hat{L}^\dagger) \right]}_{=:C(\tau)}, \end{aligned} \quad (\text{S8})$$

with  $t_k = k\delta t$ , and in the last line we defined  $\tau := t_{j-1} - t_{k+1}$ . We further adopt the convention for the time evolution of an operator  $\hat{\mathcal{O}}(t) = e^{\mathcal{L}t} \hat{\mathcal{O}}(0)$ . In the long-time limit, we assume the replacement  $\rho(t) \xrightarrow{t \rightarrow \infty} \rho_{ss}$ , which yields the expression Eq. (3) for the QFI rate and shows, that the QFI is related to the first and second intensity correlation functions [69] and independent of the true value of the parameter  $\varphi_0$ . Results for the BTC are then obtained by using  $\hat{H} = \omega \hat{S}_x$  and  $\hat{L} = \hat{S}_-$ . In the following, we will assume this choice of the Hamiltonian and jump operator if not stated otherwise, yielding the Lindblad master equation

$$\partial_t \rho = -i\omega [\hat{S}_x, \rho] + \kappa \mathcal{D}[\hat{S}_-] \rho. \quad (\text{S9})$$

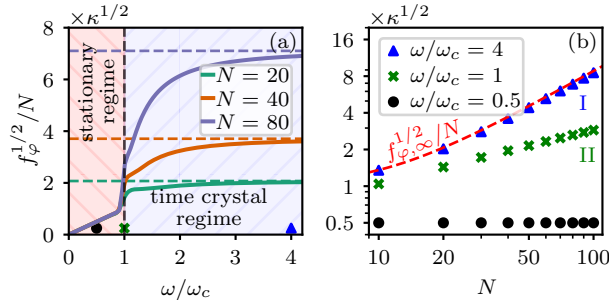


FIG. S1. **Beyond Heisenberg scaling of the QFI rate.** (a) Square root of the system size rescaled long-time limit QFI rate as a function of the Rabi frequency  $\omega$  and for varying system sizes  $N$ . The dashed lines indicate the saturating value  $f_{\varphi,\infty}$ . (b) Square root of the system size rescaled QFI rate as a function of the system size  $N$  for selected constant values of  $\omega/\omega_c$ . For I and II, the asymptotic behavior is determined by a power law fit yielding scaling behaviors of  $f_\varphi \propto N^{\alpha_i}$  with  $\alpha_I = 3.923 \pm 0.004$  and  $\alpha_{II} = 2.8417 \pm 0.0018$ . The red dashed line indicates the saturating value  $f_{\varphi,\infty}$ . For both panels, numerical values are obtained, using diagonalization of Eq. (S7) and  $f_{\varphi,\infty}$  corresponds to Eq. (4).

## TIME-CORRELATIONS IN THE SINGLE SYSTEM AND THE SUPERSPIN METHOD

In this section, we compute an approximation to the correlation function  $C(\tau)$  in the extreme time crystal limit  $\omega/\omega_c \rightarrow \infty$  of a BTC, using the superspin method developed in [70]. This method uses the vectorized form of the Lindbladian superoperator and the density matrix. This approach assumes the transformation of operators to vectors according to  $\mathcal{O} = |m\rangle\langle n| \rightarrow |\mathcal{O}\rangle = |m\rangle \otimes |n|^*$ . Applying this transformation to the Lindblad Master Equation Eq. (S9) leads to the matrix equation  $\partial_t |\rho\rangle = \tilde{\mathcal{L}} |\rho\rangle$ , with the vectorized Lindblad superoperator [70]

$$\tilde{\mathcal{L}} = \tilde{\mathcal{L}}_0 + \tilde{\mathcal{L}}_D = \underbrace{i\omega \hat{J}_x}_{\tilde{\mathcal{L}}_0} - \underbrace{\frac{\kappa}{4} \left( \hat{J}_x^2 + \hat{J}^2 \right)}_{\tilde{\mathcal{L}}_D}, \quad (\text{S10})$$

where we have defined the superspin components  $\hat{J}_\alpha = \hat{S}_\alpha \otimes \mathbf{1} - \mathbf{1} \otimes \hat{S}_\alpha$ . Since the vectorized Lindblad superoperator only depends on the total superspin and its x-projection, it is customary to use the x-superspin basis of the respective

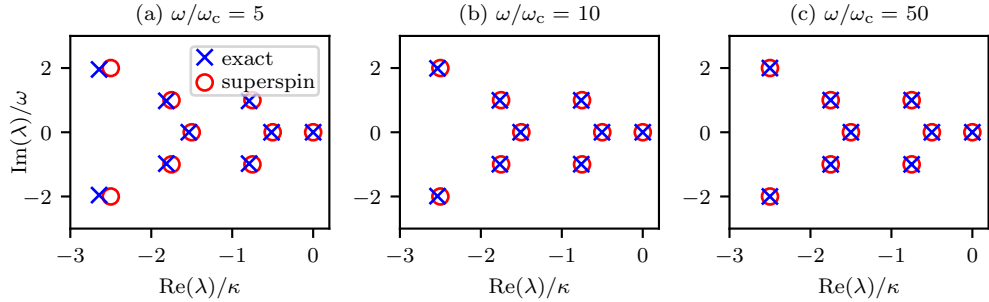


FIG. S2. **Benchmark of the superspin eigenvalue spectrum.** Comparison of the Lindbladian eigenvalues for the BTC obtained by exact diagonalization (blue crosses) and by the superspin method (red circles), for different values of the Rabi frequency  $\omega$  and system size  $N = 10$ . With increasing Rabi frequency the agreement between the approximation and the exact eigenvalues increases.

Liouville space, where the common eigensupercets can be labeled as  $|j, j_x\rangle\rangle$  [70]. We restrict the calculations to the maximally polarized sector with a BTC composed of  $N$  emitters. This implies values of  $j = 0, \dots, N$  and  $j_x = -j, \dots, j$  [70].

In the strong driving or extreme time crystal limit ( $\omega/\omega_c \rightarrow \infty$ ) and for fixed system size, the term  $\tilde{\mathcal{L}}_D$  can be considered a small perturbation of the unperturbed contribution  $\tilde{\mathcal{L}}_0$ . Using a first order perturbation calculation, we compute an approximation to the Lindbladian eigenvalues as [70]

$$\lambda_{j,j_x} = i\omega j_x - \frac{\kappa}{4}(j_x^2 + j(j+1)), \quad (\text{S11})$$

where the labels  $j, j_x$  correspond to the x-basis superspin states. We are interested in computing the correlation function  $C(\tau)$ . In the extreme time crystal limit, the stationary state approaches the maximally mixed state, i.e.  $\rho_{ss} \approx 1/(N+1)$  [83, 84]. Thus, to first order the correlation function reads [45]

$$C(\tau) \approx \sum_{j,j_x} e^{\lambda_{j,j_x}\tau} \langle\langle \hat{S}_+ \hat{S}_- | j, j_x \rangle\rangle \langle\langle j, j_x | \hat{S}_- \hat{S}_+ \rangle\rangle / (N+1), \quad (\text{S12})$$

where we used the decomposition  $e^{\mathcal{L}\tau} \approx \sum_{j,j_x} e^{\lambda_{j,j_x}\tau} |j, j_x\rangle\rangle \langle\langle j, j_x|$ . We further simplify this expression by determining the x-basis superspin states, using the rule  $\hat{J}_\alpha |\hat{O}\rangle\rangle = |[\hat{S}_\alpha, \hat{O}]\rangle\rangle$  [45, 70]. For example the state corresponding to  $j = 1, j_x = 0$  reads up to a phase

$$\hat{J}_x |\hat{S}_x\rangle\rangle = |[\hat{S}_x, \hat{S}_x]\rangle\rangle = 0 \quad (\text{S13})$$

$$\hat{J}^2 |\hat{S}_x\rangle\rangle = |[\hat{S}_y, [\hat{S}_y, \hat{S}_x]]\rangle\rangle + |[\hat{S}_z, [\hat{S}_z, \hat{S}_x]]\rangle\rangle = 2|\hat{S}_x\rangle\rangle \quad (\text{S14})$$

$$\Rightarrow |1, 0\rangle\rangle = \mathcal{N}_{1,0} |\hat{S}_x\rangle\rangle \quad (\text{S15})$$

$$\langle\langle 1, 0 | 1, 0 \rangle\rangle = \text{Tr} \left[ \hat{S}_x^2 \right] |\mathcal{N}_{1,0}|^2 \stackrel{!}{=} 1 \Rightarrow |\mathcal{N}_{1,0}| = \frac{2\sqrt{3}}{\sqrt{N(N+1)(N+2)}}. \quad (\text{S16})$$

Next, we decompose the superstates  $|\hat{S}_\pm \hat{S}_\mp\rangle\rangle$  in the  $|j, j_x\rangle\rangle$  basis by using the ladder operators in the x-basis  $\hat{S}_\pm^{(x)} = \hat{S}_y \pm i\hat{S}_z$  and applying the identity for ladder operators in the z-basis  $\hat{S}_\pm \hat{S}_\mp = \hat{S}^2 - \hat{S}_z^2 \pm \hat{S}_z$ , yielding

$$|\hat{S}_\pm \hat{S}_\mp\rangle\rangle = \underbrace{\frac{2}{3} |\hat{S}^2\rangle\rangle}_{\propto |0,0\rangle\rangle} \mp \underbrace{\frac{i}{2} \left( |\hat{S}_+^{(x)}\rangle\rangle - |\hat{S}_-^{(x)}\rangle\rangle \right)}_{\propto (|1,1\rangle\rangle - |1,-1\rangle\rangle} + \underbrace{\frac{1}{2} \left( |\hat{S}_x^2\rangle\rangle - \frac{1}{3} |\hat{S}^2\rangle\rangle \right)}_{\propto |2,0\rangle\rangle} + \underbrace{\frac{1}{4} \left( |(\hat{S}_+^{(x)})^2\rangle\rangle + |(\hat{S}_-^{(x)})^2\rangle\rangle \right)}_{\propto (|2,2\rangle\rangle + |2,-2\rangle\rangle}, \quad (\text{S17})$$

where the basis states underset in Eq. (S17) read

$$|0, 0\rangle = \frac{4}{\sqrt{N+1}N(N+2)}|\hat{S}^2\rangle, \quad (\text{S18})$$

$$|1, \pm 1\rangle = \sqrt{\frac{6}{N(N+1)(N+2)}}|\hat{S}_\pm^{(\text{x})}\rangle, \quad (\text{S19})$$

$$|2, 0\rangle = \sqrt{\frac{180}{(N-1)N(N+1)(N+2)(N+3)}}\left(|\hat{S}_\text{x}^2\rangle - \frac{1}{3}|\hat{S}^2\rangle\right), \quad (\text{S20})$$

$$|2, \pm 2\rangle = \sqrt{\frac{30}{(N-1)N(N+1)(N+2)(N+3)}}|(\hat{S}_\pm^{(\text{x})})^2\rangle, \quad (\text{S21})$$

where we chose real normalization constants. With this decomposition and the respective eigenvalues  $\lambda_{j,j_\text{x}}$ , we compute the correlation function as

$$C(\tau) \approx \frac{N^2(N+2)^2}{36} - \frac{N(N+2)}{12}e^{-3\kappa\tau/4}\cos(\omega\tau) + \frac{(N-1)N(N+2)(N+3)}{240}\left(e^{-5\kappa\tau/2}\cos(2\omega\tau) + \frac{1}{3}e^{-3\kappa\tau/2}\right). \quad (\text{S22})$$

With this expression, we compute the QFI, which yields the result in Eq. (4) in the extreme time crystal limit  $\omega/\omega_c \rightarrow \infty$ . We numerically benchmark the expressions for the first order approximated eigenvalues in Fig. S2 and the correlation function in Fig. S3.

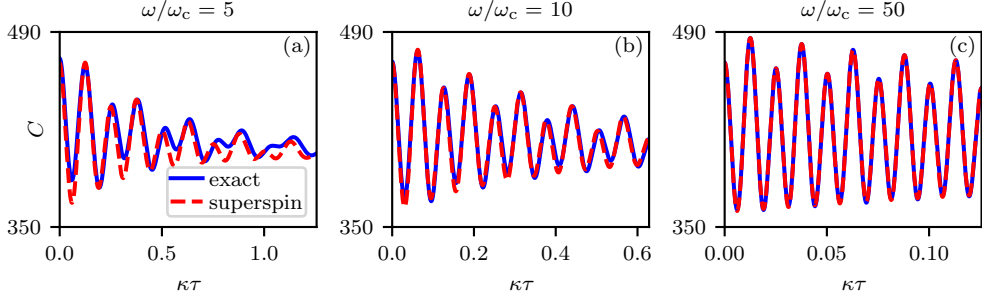


FIG. S3. **Benchmark of the superspin correlation function.** Correlation function  $C(\tau)$  as a function of time, for different Rabi frequencies  $\omega$ . In all panels, the system size is  $N = 10$ . The exact results (blue solid line) are obtained, using numerical integration of the Lindblad master equation and the superspin results (red dashed line) represent the evaluation of Eq. (S22). With increasing Rabi frequency the agreement between the superspin method and exact evolution increases.

### LARGE DEVIATIONS APPROACH TO PHOTONCOUNTING

In the main text, we consider estimation of the parameter  $\varphi$  via continuous monitoring of the decoder output intensity  $I_T = (1/T) \int_0^T dN(t)$ . The statistics of the number of photon emissions until time  $T$ ,  $M = \int_0^T dN(t)$ , are described by a Laplace transform of the probability distribution, yielding the generating function [73]

$$Z_c(s, \Delta\varphi) := \sum_{M=0}^{\infty} p_M(T, \Delta\varphi) e^{-sM}, \quad (\text{S23})$$

with the probability  $p_M(T, \Delta\varphi)$  of observing  $M$  emissions until time  $T$ . The moments of the photon count at time  $T$  are then given by derivatives of  $Z_c$ . In the long-time limit, the generating function has the large deviation form  $Z_c(s) \sim e^{T\theta_c(s, \Delta\varphi)}$  with the large deviation function  $\theta_c(s, \Delta\varphi)$  [73].  $Z_c$ ,  $p_M$  and  $\theta_c$  inherit a  $\Delta\varphi$ -dependence from Eq. (8), since the operators  $\hat{L}_{\text{casc}}$  and the stationary state  $\rho_{\text{ss}}$  depend on  $\Delta\varphi$  in the cascaded system.  $\theta_c(s, \Delta\varphi)$  is computed as the dominant eigenvalue of the tilted master equation [42, 73, 74, 85]

$$\partial_t \rho = \mathcal{L}_{\text{casc}}[\rho] + (e^{-s} - 1)\hat{L}_{\text{casc}}\rho\hat{L}_{\text{casc}}^\dagger, \quad (\text{S24})$$

with the physical Lindbladian  $\mathcal{L}_{\text{casc}}$  of the cascaded system and a bias described by  $s$ . For  $s = 0$ , Eq. (S24) generates the physical dynamics and for  $s \neq 0$  it generates an ensemble of trajectories with the bias  $e^{-sM}$  [73, 85]. The estimation error thus is approximated in terms of the large deviations function  $\theta_c(s, \Delta\varphi)$  as

$$\delta\varphi \sim \frac{\overline{\delta\varphi}}{\sqrt{T}}, \text{ with } \overline{\delta\varphi} := \frac{\sqrt{\partial_s^2\theta_c(s, \Delta\varphi)}}{|\partial_\varphi\partial_s\theta_c(s, \Delta\varphi)|} \Big|_{s=0} = \frac{\overline{\sigma_{I_T}}}{|\partial_\varphi I_T|}, \quad (\text{S25})$$

with the time rescaled standard deviation  $\overline{\sigma_{I_T}} = \sqrt{\partial_s^2\theta_c(s, \Delta\varphi)}|_{s=0}$ , and the derivative of the long-time averaged intensity  $-\partial_\varphi\partial_s\theta_c(s, \Delta\varphi)|_{s=0} = \partial_\varphi I_T$ . It follows immediately that the estimation error decreases with measurement time as  $\delta\varphi \sim 1/\sqrt{T}$ , obeying the standard quantum limit for long measurement times.

### LARGE DEVIATIONS APPROACH TO HOMODYNE DETECTION

In the main text, we consider the time averaged homodyne current  $J_T = (1/T) \int_0^T J_\beta(t) dt = K_T/T$ , with the time integrated homodyne current  $K_T$ . Its moments are determined by the generating function

$$Z_h(s, \varphi - \beta) = \int dK e^{-sK} p_K(T, \varphi - \beta), \quad (\text{S26})$$

where  $p_K(T, \varphi - \beta) = P(K_T = K)$  is the probability density of observing  $K_T = K$ . For long times  $T$ ,  $Z_h$  acquires the large deviation form  $Z_h(s) \sim e^{T\theta_h(s, \varphi - \beta)}$  [8], with the large deviation function  $\theta_h(s, \varphi - \beta)$ .  $Z_h$ ,  $p_K$  and  $\theta_h$  inherit a  $\varphi - \beta$  dependence from  $J_\beta$ .  $\theta_h$  is computed as the eigenvalue with largest real part of the deformed master equation [8]

$$\partial_t \rho = \mathcal{L}[\rho] - s\sqrt{\kappa} \left( \hat{S}_- e^{i(\beta - \varphi)} \rho + \rho \hat{S}_+ e^{-i(\beta - \varphi)} \right) + \frac{s^2}{2} \rho, \quad (\text{S27})$$

with the physical Lindbladian of a single BTC  $\mathcal{L}$ . For  $s \rightarrow 0$ , the physical evolution is recovered.  $J_T$  approaches its ensemble average in the long-time limit, as in a law of large numbers, yielding  $\lim_{T \rightarrow \infty} J_T = \lim_{T \rightarrow \infty} \mathbb{E}[J_T] = \lim_{T \rightarrow \infty} \mathbb{E}[K_T]/T = -\partial_s\theta_h(s, \varphi - \beta)$  [69], and its variance behaves as  $\lim_{T \rightarrow \infty} \mathbb{E}[J_T^2] - \mathbb{E}[J_T]^2 = \lim_{T \rightarrow \infty} \partial_s^2\theta_h(s, \varphi - \beta)/T$ . The estimation error for measuring  $\varphi$  via monitoring of the long-time averaged homodyne current thus is approximated by

$$\delta\varphi \sim \frac{\overline{\delta\varphi}}{\sqrt{T}}, \text{ with } \overline{\delta\varphi} := \frac{\sqrt{\partial_s^2\theta_h(s, \varphi - \beta)}}{|\partial_\varphi\partial_s\theta_h(s, \varphi - \beta)|} \Big|_{s=0} = \frac{\overline{\sigma_{J_T}}}{|\partial_\varphi J_T|}, \quad (\text{S28})$$

with the time rescaled standard deviation  $\overline{\sigma_{J_T}} := \sqrt{\partial_s^2\theta_h(s, \varphi - \beta)}|_{s=0}$ , the time rescaled estimation error  $\overline{\delta\varphi}$  and the derivative of the homodyne current in the long-time limit  $\partial_\varphi J_T := -\partial_\varphi\partial_s\theta_h(s, \varphi - \beta)|_{s=0}$ . Similar to the estimation error in the cascaded measurement protocol, the estimation error decreases with measurement time as  $\delta\varphi \sim 1/\sqrt{T}$ , obeying the standard quantum limit for long measurement times.

### HOLSTEIN PRIMAKOFF APPROACH TO THE SINGLE SYSTEM

In the stationary regime, we approximate the behavior of the BTC by applying the Holstein-Primakoff (HP) transformation to its spin operators. Here we follow the prescription given in [42] and express the spin operators in terms of bosonic ladder operators

$$\hat{S}_+ = \hat{b}^\dagger \sqrt{2S - \hat{b}^\dagger \hat{b}}, \quad \hat{S}_- = \sqrt{2S - \hat{b}^\dagger \hat{b}} \hat{b}, \quad (\text{S29})$$

with  $S = N/2$  as in the main text. The bosonic mode described by the operators  $\hat{b}^{(\dagger)}$  is assumed to be in a large displaced state, such that only quantum fluctuations around this large displaced state are studied

$$\hat{b} \rightarrow \hat{b} + \sqrt{S}\beta, \quad (\text{S30})$$

where  $\beta$  is a complex field, which is determined below. If  $S$  describes a large displacement, the spin operators can be expanded in the small parameter  $\epsilon = 1/\sqrt{S}$

$$\hat{m}_\alpha = \frac{\hat{S}_\alpha}{S} = \sum_{l=0}^{\infty} \epsilon^l \hat{m}_{\alpha,l}. \quad (\text{S31})$$

Explicit expressions up to order  $\mathcal{O}(\epsilon)$  are given by

$$m_{+,0} = \sqrt{k}\beta^* \text{ and } \hat{m}_{+,1} = \frac{1}{2\sqrt{k}}[(4 - 3|\beta|^2)\hat{b}^\dagger - \beta^{*2}\hat{b}], \quad (\text{S32})$$

where  $k = 2 - |\beta|^2$ . The field  $\beta$  is then determined by inserting the expanded operators in the Lindblad master equation. However, it is helpful to account for the physical behaviour of the system before. The critical frequency scales with the system size as  $\omega_c = N\kappa/2 = S\kappa$ . This extensive character of the Rabi frequency is accounted for by rescaling according to

$$\omega = \tilde{\omega}S, \quad \tau = St, \quad (\text{S33})$$

where also the time scale of the dynamics is rescaled. With the rescaled operators and parameters, the Lindblad master equation is obtained

$$\partial_\tau \rho = -i\tilde{\omega}S[\hat{m}_x, \rho] + \kappa S \left( \hat{m}_- \rho \hat{m}_+ - \frac{1}{2} \{ \hat{m}_+ \hat{m}_-, \rho \} \right). \quad (\text{S34})$$

By expanding the density matrix  $\rho = \sum_{l=0}^{\infty} \epsilon^l \rho_l$  and setting the right-hand side of Eq. (S34) equal to zero, we obtain the field  $\beta$  in the stationary state. Up to  $\mathcal{O}(\epsilon)$ , this yields

$$0 = -i\tilde{\omega} \pm \kappa m_{\pm,0} \Rightarrow \beta \sqrt{2 - |\beta|^2} = -i\frac{\tilde{\omega}}{\kappa}, \quad (\text{S35})$$

from which  $\beta$  is determined to  $\beta = -i\sqrt{1 - \sqrt{1 - (\tilde{\omega}/\kappa)^2}}$ . This is only valid in the regime where  $\tilde{\omega} \leq \kappa$ , i.e. the stationary regime. For the dominant order of the rescaled ladder operators, we obtain

$$m_{\pm,0} = \pm \frac{i\tilde{\omega}}{\kappa}. \quad (\text{S36})$$

The term of  $\mathcal{O}(1)$  of the rescaled Lindblad master equation yields

$$\partial_\tau \rho_0 = \kappa \left( \hat{m}_{-,1} \rho_0 \hat{m}_{+,1} - \frac{1}{2} \{ \hat{m}_{+,1} \hat{m}_{-,1}, \rho_0 \} \right), \quad (\text{S37})$$

which we solve for the stationary state by the ansatz  $\rho_{0,\text{ss}} = |E_0\rangle\langle E_0|$ , where the state  $|E_0\rangle$  is annihilated by the fluctuation of the lowering operator  $\hat{m}_{-,1}$ . By expanding  $\hat{m}_{-,1} = A\hat{b} + B\hat{b}^\dagger$  with the coefficients

$$A = \frac{1 + 3\sqrt{1 - (\tilde{\omega}/\kappa)^2}}{2\sqrt{1 + \sqrt{1 - (\tilde{\omega}/\kappa)^2}}}, \quad B = \frac{1 - \sqrt{1 - (\tilde{\omega}/\kappa)^2}}{2\sqrt{1 + \sqrt{1 - (\tilde{\omega}/\kappa)^2}}}, \quad (\text{S38})$$

we arrive at the stationary state

$$|E_0\rangle = \frac{1}{\sqrt{\mathcal{N}}} |0\rangle + \frac{1}{\sqrt{\mathcal{N}}} \sum_{n=1}^{\infty} (-1)^n \left( \frac{B}{A} \right)^n \sqrt{\frac{(2n-1)!!}{2n!!}} |2n\rangle. \quad (\text{S39})$$

$\mathcal{N}$  is a normalization constant and  $|n\rangle$  is a Fock state in the bosonic mode. Note, that this is only well defined for  $|B/A| \leq 1$  and in the stationary regime  $\tilde{\omega} < \kappa$ , meaning that the given HP approach is only valid in the stationary regime.

## Calculation of the QFI

In order to determine an expression for the QFI, we analyze the deformed master equation Eq. (S7). Inserting the rescaled operators and parameters yields the rescaled deformed master equation

$$\partial_\tau \rho = \mathcal{L}[\rho] + (e^{-i\Delta\varphi} - 1) \kappa S \hat{m}_- \rho \hat{m}_+. \quad (\text{S40})$$

We make an ansatz for the dominant eigenstate similar to the undeformed master equation as

$$\rho_0 = |E_0^{\varphi_1}\rangle\langle E_0^{\varphi_2}|. \quad (\text{S41})$$

$|E_0^\varphi\rangle$  denotes the stationary state of the fluctuations  $\hat{m}_{-,1}$  as in Eq. (S39), evaluated at the point  $\varphi$ . As this state is independent of  $\varphi$ , one could neglect the superscript, but it is carried here in order to keep the notation consistent with situations, where the stationary state depends on the estimated parameter [42]. We expand the action of  $\hat{m}_-$  as

$$\hat{m}_- |E_0^{\varphi_1}\rangle = \left( m_{-,0}^{\varphi_1} + \frac{1}{\sqrt{S}} \hat{m}_{-,1}^{\varphi_1} + \dots \right) |E_0^{\varphi_1}\rangle \text{ and } \langle E_0^{\varphi_2}| \hat{m}_- = \langle E_0^{\varphi_2} | \left( m_{-,0}^{\varphi_2} + \frac{1}{\sqrt{S}} \hat{m}_{-,1}^{\varphi_2} + \dots \right). \quad (\text{S42})$$

With this ansatz, the deformed master equation yields

$$\partial_\tau \rho_0 = \mathcal{L}[\rho_0] + (e^{-i\Delta\varphi} - 1) \kappa S \left( m_{-,0}^{\varphi_1} + \frac{1}{\sqrt{S}} \hat{m}_{-,1}^{\varphi_1} + \dots \right) |E_0^{\varphi_1}\rangle\langle E_0^{\varphi_2}| \left( m_{-,0}^{\varphi_2} + \frac{1}{\sqrt{S}} \hat{m}_{-,1}^{\varphi_2} + \dots \right), \quad (\text{S43})$$

with  $\Delta\varphi := \varphi_1 - \varphi_2$  and  $m_{\pm,0}^\varphi = m_{\pm,0} = \pm i\tilde{\omega}/\kappa$  as before. Of interest are the derivatives of the dominant eigenvalue of this tilted master equation,  $\lambda_0(\Delta\varphi)$ . The contribution  $\mathcal{L}[\rho_0]$  vanishes due to  $\hat{m}_{-,1}^\varphi |E_0^\varphi\rangle = 0$ . The leading contribution to  $\lambda_0$  reads

$$(e^{-i\Delta\varphi} - 1) \kappa S m_{-,0}^{\varphi_1} m_{+,0}^{\varphi_2} |E_0^{\varphi_1}\rangle\langle E_0^{\varphi_2}| = (e^{-i\Delta\varphi} - 1) \kappa S \underbrace{\frac{\tilde{\omega}^2}{\kappa^2} \rho_0}_{=: \tilde{\lambda}_0(\varphi_1, \varphi_2)} = \underbrace{(e^{-i\Delta\varphi} - 1) S \frac{\tilde{\omega}^2}{\kappa} \rho_0}_{=: \tilde{\lambda}_0(\varphi_1, \varphi_2)}. \quad (\text{S44})$$

The next-to-dominant term vanishes, because  $\hat{m}_{-,1}^\varphi |E_0^\varphi\rangle = 0$ . Thus, one finds for the dominant eigenvalue of the deformed master equation in leading order,  $\lambda_0(\Delta\varphi) = S\tilde{\lambda}_0(\Delta\varphi)$ , where the factor of  $S$  comes from the previous rescalings Eq. (S33). This expression is benchmarked with results from diagonalization of Eq. (S7) in Fig. S4. In the stationary regime, the QFI rate in the long-time limit thus has the compact form

$$f_\varphi = \lim_{T \rightarrow \infty} \frac{F_\varphi(\varphi, T)}{T} = 4\partial_{\varphi_1}\partial_{\varphi_2}\lambda_0|_{\varphi_1=\varphi_2} = 4\partial_{\varphi_1}\partial_{\varphi_2} \left( e^{-i(\varphi_1-\varphi_2)} - 1 \right) \frac{S^2\tilde{\omega}^2}{\kappa}|_{\varphi_1=\varphi_2} = 4\frac{\omega^2}{\kappa}. \quad (\text{S45})$$

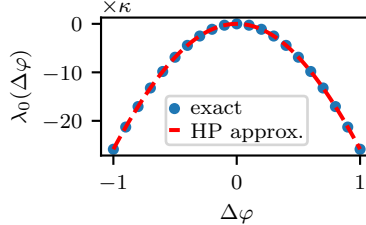


FIG. S4. **Benchmark of the HP approximation for the QFI.** Dominant eigenvalue of Eq. (S7) as a function of the phase difference  $\Delta\varphi = \varphi_1 - \varphi_2$ . Comparison of the dominant eigenvalue  $\lambda_0$  computed via exact diagonalization Eq. (S7) (blue dots) and the HP approximation Eq. (S45) (red dashed line), for  $N = 30$ , and in the stationary regime  $\omega/\omega_c = 0.5$ .

## Estimation error for the homodyne protocol

Here, we compute an approximation to the estimation error of the parameter  $\varphi$  via homodyne detection, using the HP approach. With the rescaled parameters Eq. (S33) and the expanded operators Eq. (S31), the deformed master equation for the homodyne current Eq. (S27) reads

$$\partial_\tau \rho = \mathcal{L}[\rho] + s\sqrt{\kappa} \left( \hat{m}_- e^{i(\beta-\varphi)} \rho + \rho \hat{m}_+ e^{-i(\beta-\varphi)} \right) + \frac{s^2}{2} \frac{\rho}{S}. \quad (\text{S46})$$

As an ansatz for the dominant eigensatate we choose the vacuum of the fluctuations  $\rho_0 = |E_0\rangle\langle E_0|$ . Inserting on the right hand side and using the relations Eq. (S36) yields to leading order

$$\begin{aligned} s\sqrt{\kappa} \left\{ e^{i(\beta-\varphi)} (m_{-,0} + \hat{m}_{-,1} + \dots) \rho_0 + \rho_0 (m_{+,0} + \hat{m}_{+,1} + \dots) e^{-i(\varphi-\beta)} \right\} + \frac{s^2}{2} \frac{\rho_0}{S} \\ \approx s\sqrt{\kappa} \frac{i\tilde{\omega}}{\kappa} \left( e^{-i(\beta-\varphi)} - e^{i(\beta-\varphi)} \right) \rho_0 + \frac{s^2}{2} \frac{\rho_0}{S}, \end{aligned} \quad (\text{S47})$$

where we included the term  $s^2/(2S)$ , since it defines the variance of the homodyne current, but neglected terms with  $\hat{m}_{\pm,2}$ , which are also of  $\mathcal{O}(\epsilon^2)$ , but only contribute to the  $-\partial_s \partial_\varphi \theta_h$  term in the estimation error, where they are subdominant to  $\mathcal{O}(1)$  terms. Thus, the dominant eigenvalue of the rescaled deformed master equation reads

$$\tilde{\theta}_h(s, \varphi - \beta) = 2s \frac{\omega}{S\sqrt{\kappa}} \sin(\beta - \varphi) + \frac{s^2}{2S}, \quad (\text{S48})$$

where, due to the rescaling of Eq. (S27),  $\theta_h(s, \varphi - \beta) = S\tilde{\theta}_h(s, \varphi - \beta)$ . For the estimation error, this means

$$\overline{\delta\varphi} = \sqrt{\frac{\partial_s^2 \theta_h(s, \varphi - \beta)}{(\partial_\varphi \partial_s \theta_h(\tilde{s}, \varphi - \beta))^2}} \Big|_{\tilde{s}=0} = \frac{\sqrt{\kappa}}{2\omega |\cos(\beta - \varphi)|}. \quad (\text{S49})$$

This result is numerically benchmarked with results from diagonalization of Eq. (S27) as shown in Fig. S5.

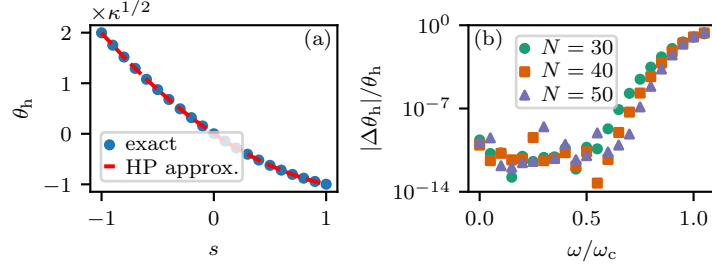


FIG. S5. **Benchmark of the HP approximation for the homodyne protocol.** (a) Dominant eigenvalue of Eq. (S27) as a function of the bias parameter  $s$  for  $\varphi - \beta = 0.1$ , fixed system size  $N = 30$ , and in the stationary regime  $\omega/\omega_c = 0.5$ . Comparison of values obtained by exact diagonalization of Eq. (S27) (blue dots) and evaluation of Eq. (S48) (red dashed line). (b) Relative error of the dominant eigenvalue  $\theta_h$  as a function of the Rabi frequency  $\omega$ , for different system sizes, and fixed values  $\varphi - \beta = 0.1$  and  $s = -0.05$ . The error is defined as the absolute difference of the HP approximated value and the exact diagonalized value, divided by the exact value. One observes that the error increases towards the critical Rabi frequency, but is small in a large portion of the stationary regime.

## CONSTRUCTION OF THE OPTIMAL DECODER IN THE STATIONARY REGIME

This section follows the construction of an optimal decoder presented in [63]. We show, how the perfect absorber protocol emerges from this construction as the optimal measurement protocol in the stationary regime. We assume here a matrix product (MP) description of the cascaded source-decoder system, where we access the trajectory of emissions  $\{i_1, \dots, i_n\}$  in small but finite time bins of size  $\delta t$  over a measurement time  $T = n\delta t$  by continuously monitoring the decoder output. This is formally implemented by the measurement

$$\Pi_{\{i_j\}}^{\text{DE}} = U_{\text{DE}}^\dagger(T) \Pi_{\{i_j\}} U_{\text{DE}}(T), \quad (\text{S50})$$

acting on the decoder and emission field state  $\rho_D(0) \otimes \rho_E(T)$  before their interaction.  $\rho_D(0) = |\chi_D(0)\rangle\langle \chi_D(0)|$  is the decoder initial state and  $\rho_E(T)$  describes the emission field at time  $T$ , after the interaction with the source.  $\Pi_{\{i_j\}} = \bigotimes_{j=1}^n |i_j\rangle\langle i_j|$  is the projector on the observed trajectory in the basis of the source and decoder emission field time bin modes, interacting sequentially with the source and decoder [86].  $U_{\text{DE}}$  is a unitary, describing the joint evolution of the decoder and emission field. In the MP description of the decoder and emission field state, this unitary is a MP Operator (MPO). The resulting measurement  $\Pi_{\{i_j\}}^{\text{DE}}$  thus inherits a MP structure.

The global system and emission field state is a pure MPS,  $|\psi_\varphi\rangle$ , with the true value  $\varphi$  inscribed. Any projective measurement  $\{\Pi_k^{\text{SE}}\}$  of the state  $|\psi_\varphi\rangle$  containing the projector  $\Pi_0^{\text{SE}} = |\psi_\varphi\rangle\langle \psi_\varphi|$  is optimal [68, 87–89] in the vicinity

of  $\varphi'$ , in the sense that it saturates the QCRB evaluated at  $\varphi'$ . By tuning  $\varphi'$  to  $\varphi' = \varphi$ , the projective measurement  $\{\Pi_k^{\text{SE}}\}$  becomes optimal for the true realization of  $\varphi$ . For  $\Pi_{\{i_j\}}^{\text{DE}}$  to be optimal, it has to obey the same emission field structure as  $\Pi_0^{\text{SE}}$  for at least one specific trajectory  $\{m_j\}$ , yielding the condition

$$U_{\text{DE}}(\varphi', T) [\Pi_0^{\text{SE}} \otimes \rho_D(0)] U_{\text{DE}}^\dagger(\varphi', T) = \Pi_{\{m_j\}} \otimes \rho_{\text{SD}}(\varphi', T). \quad (\text{S51})$$

Physically, the unitary  $U_{\text{DE}}(\varphi', T)$  transforms the source and emission field state  $\Pi_0^{\text{SE}}$  into the specific trajectory  $\{m_j\}$  of the emission field as described by the projector  $\Pi_{\{m_j\}}$ , for  $\varphi = \varphi'$ . In this transformation the source and decoder evolve into a general state  $\rho_{\text{SD}}(\varphi', T)$ , which is discarded.  $U_{\text{DE}}$  and  $\rho_{\text{SD}}$  inherit a dependence on  $\varphi'$  from  $\Pi_0^{\text{SE}}$ . A convenient choice for the target trajectory is the vacuum  $\{m_j\} = \{0, 0, \dots, 0\}$ , which describes a dark decoder output and renders the decoder a perfect absorber.

A general construction of a decoder satisfying Eq. (S51) can be challenging. However, in the long-time limit, a convenient construction can be found, if the source evolves according to a time-homogeneous master equation with support for a stationary state  $\rho_{S,ss} = \sum_{k=1}^d p_{k,ss}(\varphi') |k_{ss}(\varphi')\rangle_S \langle k_{ss}(\varphi')|$  at a parameter value  $\varphi'$ . In the stationary regime ( $\omega < \omega_c$ ), the source stationary state is well approximated by the pure stationary state  $\rho_{S,ss} = |E_0\rangle_S \langle E_0|$  [see Eq. (S39)]. In such a situation, the prescription for the decoder operators given in [63] simplifies to  $\hat{H}_D = -W_0 \hat{H}_S(\varphi') W_0^\dagger$  and  $\hat{L}_D = -W_0 \hat{L}_S(\varphi') W_0^\dagger$ , in the sense that their matrix elements with respect to the source stationary state  $|E_0\rangle_S$  and decoder stationary state  $|E_0\rangle_D = W_0 |E_0\rangle_S$  are equal. The decoder is assumed to have the same Hilbert space dimension as the source, and  $W_0$  is an arbitrary unitary. The stationary state of the source-decoder system then reads  $|\psi\rangle = |E_0\rangle_S \otimes |E_0\rangle_D$ . At  $\varphi = \varphi'$ , this state is a pure dark state, as is shown in [42]. With the choice

$$W_0 = \exp[i\pi \hat{S}_z^S], \quad (\text{S52})$$

the decoder operators are  $\hat{H}_D = \omega \hat{S}_x^D$  and  $\hat{L}_D = \kappa e^{-i\varphi'} \hat{S}_\alpha^D$ , with  $\hat{S}_\alpha^D$  acting on the decoder Hilbert space and  $\hat{S}_\alpha^S$  on the source Hilbert space. This means, that the optimal decoder is an identical copy of the source with a phase shift  $\varphi'$  imprinted on emitted photons.

## HOLSTEIN PRIMAKOFF APPROACH TO THE SOURCE-DECODER SYSTEM

In this section, the HP approach is taken to the cascaded source-decoder system, to obtain an analytical expression for the estimation error  $\delta\varphi$  in the cascaded stationary regime ( $\omega < \omega_{c,\text{casc}}$ ) similar to [42]. We start as before with the HP transformation

$$\hat{S}_+^i = \hat{b}_i^\dagger \sqrt{2S - \hat{b}_i^\dagger \hat{b}_i}, \quad \hat{S}_-^{(i)} = \sqrt{2S - \hat{b}_i^\dagger \hat{b}_i} \hat{b}_i, \quad (\text{S53})$$

where the index  $i$  indicates the operators of the source ( $i = S$ ) and of the decoder ( $i = D$ ). Assuming a large displaced state for both subsystems, we shift the bosonic modes as  $\hat{b}_i \rightarrow \hat{b}_i + \sqrt{S} \beta_i$ , where the  $\beta_i$  are complex fields yet to be determined. As  $S$  is a large displacement, we expand all operators in the small parameter  $\epsilon = 1/\sqrt{S}$

$$\hat{m}_\alpha^i = \frac{\hat{S}_\alpha^i}{S} = \sum_{l=0}^{\infty} \epsilon^l \hat{m}_{\alpha,l}^i. \quad (\text{S54})$$

Similar to the case of a single system, the first order expansion reads

$$\hat{m}_+^i = m_{+,0}^i + \underbrace{\epsilon \frac{1}{2\sqrt{k_i}} [(4 - 3|\beta_i|^2) - |\beta_i|^2] \hat{b}_i^\dagger - \beta_i^{*2} \hat{b}_i}_{\hat{m}_{+,1}^i} + \mathcal{O}(\epsilon^2), \quad (\text{S55})$$

where  $k_i = 2 - |\beta_i|^2$  and  $m_{+,0}^i = \beta_i^* \sqrt{k_i}$ . Inserting the rescaled operators and rescaled parameters Eq. (S33) in the Lindblad master equation for the cascaded system yields

$$\partial_\tau \rho_{\text{ss}} = -iS\tilde{\omega}[\hat{m}_x^S + \hat{m}_x^D, \rho_{\text{ss}}] - \frac{\kappa}{2} S [e^{-i\Delta\varphi} \hat{m}_+^D \hat{m}_-^S - e^{i\Delta\varphi} \hat{m}_+^S \hat{m}_-^D, \rho_{\text{ss}}] + \kappa S \mathcal{D}[e^{-i\varphi} \hat{m}_-^S + e^{-i\varphi'} \hat{m}_-^D] \rho_{\text{ss}} \stackrel{!}{=} 0, \quad (\text{S56})$$

which we want to solve for the stationary state  $\rho_{ss}$ . By expanding the density matrix  $\rho = \sum_{l=0}^{\infty} \epsilon^l \rho_l$ , we find up to order  $\mathcal{O}(\epsilon)$  self-consistency relations

$$m_{\pm,0}^S = \pm \frac{i\tilde{\omega}}{\kappa}, \quad m_{\pm,0}^D = \pm \frac{i\tilde{\omega}}{\kappa} (1 - 2e^{\pm i\Delta\varphi}). \quad (\text{S57})$$

With the solution for the zero order moments of the ladder operators, we determine the fields  $\beta_i$  as

$$\beta_S = -i\sqrt{1 - \sqrt{1 - (\tilde{\omega}/\kappa)^2}}, \quad \beta_D = -\frac{i\tilde{\omega}}{\kappa} \frac{1 - 2e^{-i\Delta\varphi}}{\sqrt{1 + \sqrt{1 - (\tilde{\omega}^2/\kappa^2)(5 - 4\cos(\Delta\varphi))}}}. \quad (\text{S58})$$

This solution is only valid in the regime  $\tilde{\omega}^2 \leq \kappa^2/(5 - 4\cos(\Delta\varphi))$  or in other terms, we obtain an additional transition line for the cascaded system along  $\omega_{c,\text{casc}} = \omega_c/\sqrt{5 - 4\cos(\Delta\varphi)}$ , with the single system critical frequency  $\omega_c$ . The next to leading order term yields

$$\partial_\tau \rho_0 = -\frac{\kappa}{2} [e^{-i\Delta\varphi} \hat{m}_{+,1}^D \hat{m}_{-,1}^S - e^{i\Delta\varphi} \hat{m}_{+,1}^S \hat{m}_{-,1}^D, \rho_0] + \kappa \mathcal{D} [e^{-i\varphi} \hat{m}_{-,1}^S + e^{-i\varphi'} \hat{m}_{-,1}^D] \rho_0 \stackrel{!}{=} 0. \quad (\text{S59})$$

We solve this by the ansatz

$$\rho_{0,ss} = (|E_0^S\rangle \otimes |E_0^D\rangle) (\langle E_0^S| \otimes \langle E_0^D|), \quad (\text{S60})$$

with the vacuum of the fluctuations  $\hat{m}_{-,1}^i |E_0^i\rangle = 0$ . By writing out the fluctuations as  $\hat{m}_{-,1}^i = A_i \hat{b}_i + B_i \hat{b}_i^\dagger$  with

$$B_S = -\frac{1 - \sqrt{1 - \tilde{\omega}^2/\kappa^2}}{2\sqrt{k_S}}, \quad A_S = \frac{1 + 3\sqrt{1 - \tilde{\omega}^2/\kappa^2}}{2\sqrt{k_S}}, \quad (\text{S61})$$

$$B_D = \frac{(-i\tilde{\omega}/\kappa)1 - 2e^{i\Delta\varphi}}{\sqrt{1 + \sqrt{1 - (\tilde{\omega}^2/\kappa^2)(5 - 4\cos(\Delta\varphi))}\sqrt{2k_D}}}, \quad A_D = \frac{1 + 3\sqrt{1 - (\tilde{\omega}^2/\kappa^2)(5 - 4\cos(\Delta\varphi))}}{2\sqrt{k_D}}, \quad (\text{S62})$$

the explicit form of the stationary state is determined. Notice that  $|B_i/A_i| \leq 1$  and thus we find the vacuum states of the respective fluctuations

$$|E_0^i\rangle = \frac{1}{\sqrt{\mathcal{N}}} \left( |0\rangle_i + \sum_{n=1}^{\infty} \left( \frac{-B_i}{A_i} \right)^n \sqrt{\frac{(2n-1)!!}{2n!!}} |2n\rangle_i \right). \quad (\text{S63})$$

### Estimation error for the perfect absorber protocol in the stationary regime

Inserting the rescaled parameters Eq. (S33) and operators Eq. (S54) in the tilted master equation Eq. (S24) yields

$$\partial_\tau \rho = \mathcal{L}[\rho] + \kappa S(e^{-s} - 1)(e^{-i\varphi} \hat{m}_-^S + e^{-i\varphi'} \hat{m}_-^D) \rho (e^{i\varphi} \hat{m}_+^S + e^{i\varphi'} \hat{m}_+^D). \quad (\text{S64})$$

For the dominant eigenstate we choose the ansatz as in Eq. (S60),  $\rho_{0,ss} = (|E_0^S\rangle \otimes |E_0^D\rangle) (\langle E_0^S| \otimes \langle E_0^D|)$ . Inserting this ansatz on the right hand side and only considering the leading terms in the expansion of the operators yields the dominant eigenvalue

$$\begin{aligned} \theta_c(s, \Delta\varphi) &\approx \kappa S^2 (e^{-s} - 1) (m_{-,0}^S m_{+,0}^S + m_{-,0}^D m_{+,0}^D + e^{-i\Delta\varphi} m_{-,0}^S m_{+,0}^D + e^{i\Delta\varphi} m_{-,0}^D m_{+,0}^S) \\ &= S^2 (e^{-s} - 1) \frac{\tilde{\omega}^2}{\kappa} 2(1 - \cos(\Delta\varphi)) = 2(e^{-s} - 1) \frac{\omega^2}{\kappa} (1 - \cos(\Delta\varphi)), \end{aligned} \quad (\text{S65})$$

which is benchmarked with data obtained by diagonalization of Eq. (S24) in Fig. S6. From this, the estimation error is computed as

$$\overline{\delta\varphi} = \frac{\sqrt{\partial_s^2 \theta_c(s, \Delta\varphi)}}{|\partial_\varphi \partial_s \theta_c(s, \Delta\varphi)|} \Big|_{s=0} = \frac{\sqrt{\kappa(1 - \cos(\Delta\varphi))}}{\sqrt{2\omega} |\sin(\Delta\varphi)|}, \quad (\text{S66})$$

which is minimal and saturates the QCRB for  $\Delta\varphi = 0$ . Note, that this approximation only holds in the cascaded stationary regime for  $\omega < \omega_{c,\text{casc}}$ .

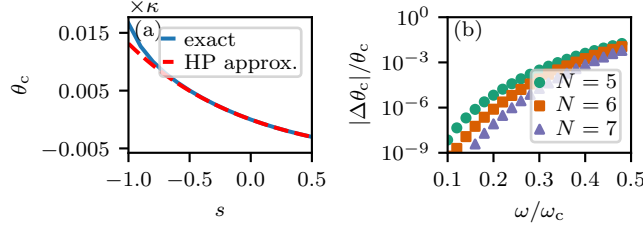


FIG. S6. **Benchmark of the HP approximation for the perfect absorber protocol.** (a) Dominant eigenvalue of Eq. (S24) as a function of the bias parameter  $s$ , for  $\Delta\varphi = 0.1$ , fixed system size  $N = 5$  and in the stationary regime  $\omega/\omega_c = 0.35$ . Comparison of results obtained with the HP approximation (red dashed line) and numerical diagonalization of Eq. (S24) (blue solid line). (b) Relative error of the dominant eigenvalue  $\theta_c$  as a function of the Rabi frequency  $\omega$ , for different system sizes, and fixed values  $\Delta\varphi = 0.1$  and  $s = -0.05$ . The error is defined as the absolute difference of the HP approximated value and the exact diagonalized value and both divided by the exact value. The error increases towards the critical Rabi frequency, but is small in a large portion of the stationary regime. The approximation improves with increasing system size.

### Mean-field operators for the source-decoder system

We define the rescaled operators as  $\hat{m}_\alpha^{i,N} = 2\hat{S}_\alpha^i/N$ , with  $\alpha \in \{x, y, z\}$  and  $(i = S)$  for the source and  $(i = D)$  for the decoder. In the limit  $N \rightarrow \infty$ , these operators converge to multiples of the identity, i.e.  $\lim_{N \rightarrow \infty} \hat{m}_\alpha^{i,N} = \lim_{N \rightarrow \infty} \langle \hat{m}_\alpha^{i,N} \rangle =: m_\alpha^i$  [27, 90, 91]. As in the main text we consider the maximally polarized sector with total angular momentum of the subsystems  $S = N/2$ . While the time evolution of the density matrix is given by a Lindblad master equation, the evolution of expectation values is given by an adjoint Lindblad master equation

$$\begin{aligned} \partial_t \langle \hat{m}_\alpha^N \rangle = & -i\omega \left\langle \left[ \hat{m}_\alpha^N, \hat{S}_x^S + \hat{S}_x^D \right] \right\rangle - \frac{\kappa}{2} \left\langle \left[ \hat{m}_\alpha^N, e^{-i\Delta\varphi} \hat{S}_+^D \hat{S}_-^S - e^{i\Delta\varphi} \hat{S}_+^S \hat{S}_-^D \right] \right\rangle \\ & + \kappa \left\langle \left( e^{i\varphi} \hat{S}_+^S + e^{i\varphi'} \hat{S}_+^D \right) \hat{m}_\alpha^N \left( e^{-i\varphi} \hat{S}_-^S + e^{-i\varphi'} \hat{S}_-^D \right) \right\rangle \\ & - \frac{\kappa}{2} \left\langle \left\{ \left( e^{i\varphi} \hat{S}_+^S + e^{i\varphi'} \hat{S}_+^D \right) \left( e^{-i\varphi} \hat{S}_-^S + e^{-i\varphi'} \hat{S}_-^D \right), \hat{m}_\alpha^N \right\} \right\rangle. \end{aligned} \quad (\text{S67})$$

In a first step, this yields the equations of motion for the expectation values  $\langle \hat{m}_\alpha^{i,N} \rangle$ . We then continue by defining  $\omega_c = N\kappa/2$ , and rescaling time and the Rabi frequency as  $\tau = St, \omega = S\tilde{\omega}$ . With this rescaling, we then take the thermodynamic limit, assuming that expectation values factor as  $\langle \hat{m}_\alpha^{i,N} \hat{m}_\beta^{j,N} \rangle \xrightarrow{N \rightarrow \infty} \langle \hat{m}_\alpha^{i,N} \rangle \langle \hat{m}_\beta^{j,N} \rangle$ . With this we find the equations of motion

$$\partial_\tau m_x^S = \kappa m_x^S m_z^S \quad (\text{S68})$$

$$\partial_\tau m_y^S = -\tilde{\omega} m_z^S + \kappa m_y^S m_z^S \quad (\text{S69})$$

$$\partial_\tau m_z^S = \tilde{\omega} m_y^S - \kappa [(m_x^S)^2 + (m_y^S)^2] \quad (\text{S70})$$

$$\partial_\tau m_x^D = \kappa [m_x^D m_z^D + 2m_x^S m_z^D \cos(\Delta\varphi) - 2m_y^S m_z^D \sin(\Delta\varphi)] \quad (\text{S71})$$

$$\partial_\tau m_y^D = -\tilde{\omega} m_z^D + \kappa [m_z^D m_y^D + 2m_x^S m_z^D \sin(\Delta\varphi) + 2m_y^S m_z^D \cos(\Delta\varphi)] \quad (\text{S72})$$

$$\begin{aligned} \partial_\tau m_z^D = & \tilde{\omega} m_y^D - 2\kappa [(m_x^S m_z^D + m_y^S m_z^D) \cos(\Delta\varphi) + (m_x^S m_y^D - m_y^S m_x^D) \sin(\Delta\varphi)] \\ & - \kappa [(m_x^D)^2 + (m_y^D)^2]. \end{aligned} \quad (\text{S73})$$

The operators  $(\hat{m}^i)^2$  commute with all components of the angular momentum, meaning that the expectation values  $\langle (\hat{m}^i)^2 \rangle$  are conserved, and due to the maximum polarization condition  $(\hat{S}^i)^2 = N/2$ , we find  $(m^i)^2 = 1$ . Using this boundary condition, we numerically compute the dynamics generated by Eqs. (S68 - S73) for three different ratios  $\tilde{\omega}/\kappa$  and display the results for the  $m_z^i$  components in Fig. S7. We further determine the values of  $m_\pm^i$  in the thermodynamic limit and in the stationary state. By setting Eqs. (S68 - S73) to zero, we determine the stationary solutions for the mean field observables as

$$0 = m_x^S, m_y^S = \frac{\tilde{\omega}}{\kappa} \Rightarrow m_\pm^S = \pm i \frac{\tilde{\omega}}{\kappa} \quad (\text{S74})$$

$$0 = \mp i\tilde{\omega} + \kappa m_\pm^D + 2\kappa m_x^S e^{\pm i\Delta\varphi} \pm 2i\kappa m_y^S e^{\pm i\Delta\varphi} \Rightarrow m_\pm^D = \pm i \frac{\tilde{\omega}}{\kappa} - 2m_\pm^S e^{\pm i\Delta\varphi} = \pm i \frac{\tilde{\omega}}{\kappa} (1 - 2e^{\pm i\Delta\varphi}), \quad (\text{S75})$$

which agrees with the results obtained with the HP approach for  $m_{\pm,0}^i$  in Eq. (S57).

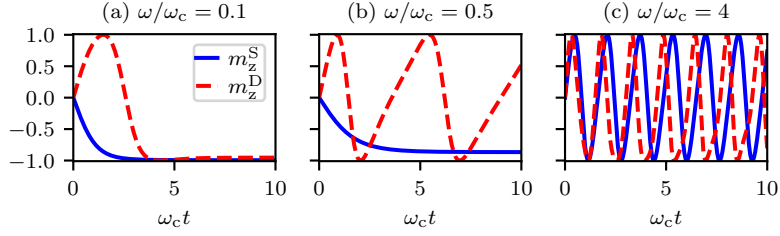


FIG. S7. **Cascaded system mean field quantities.** Mean field expectation value of the z-magnetization  $\lim_{N \rightarrow \infty} (2/N) \langle \hat{S}_z^i \rangle = m_z^i$ , with  $i = S$  for the source (blue solid line) and  $i = D$  the decoder (red dashed line), for different positions in the phase diagram.  $\omega_c = N\kappa/2$  is the critical frequency and both  $\omega$  and  $t$  are measured in units of  $\omega_c$  to obtain a well-defined limit. For all panels,  $\Delta\varphi = \pi$ . (a)  $\omega/\omega_c = 0.1$ , with source and decoder in the stationary regime. (b)  $\omega/\omega_c = 0.5$ , with the source in the stationary regime and the decoder displaying time crystal behavior. (c)  $\omega/\omega_c = 4$ , with both source and decoder in the time crystal regime.